Regd. No. C-3911

VOL. 35

INDIAN JOURNAL OF PHYSICS

No. 2

(Published in collaboration with the Indian Physical Society)

AND

VOL. 44

PROCEEDINGS

No. 2

OF THE

INDIAN ASSOCIATION FOR THE CULTIVATION OF SCIENCE

FEBRUARY 1961

PUBLISHED BY THE

INDIAN ASSOCIATION FOR THE CULTIVATION OF SCIENCE

JADAVPUR, CALCUTTA 32

Annual Subscription—
Inland Rs. 25.00
Foreign £ 2-10-0 or $ 7.00

NOTICE

TO INTENDING AUTHORS

1. Manuscripts for publication should be sent to the Assistant Editor, Indian Journal of Physics, Jadavpur, Calcutta-32.

2. The manuscripts submitted must be type-written with double space on thick foolscap paper with sufficient margin on the left and at the top. The original copy, and not the carbon copy, should be submitted. Each paper must contain an Abstract at the beginning.

3. All References should be given in the text by quoting the surname of the author, followed by year of publication, *e.g.*, (Roy, 1958). The full Reference should be given in a list at the end, arranged alphabatically, as follows; Mazumder, M. 1959, *Ind. J. Phys.*, **33**, 346.

4. Line diagrams should be drawn on white Bristol board or tracing paper with black Indian ink, and letters and numbers inside the diagrams should be written neatly in capital type with Indian ink. The size of the diagrams submitted and the lettering inside should be large enough so that it is legible after reduction to one-third the original size. A simple style of lettering such as gothic, with its uniform line width and no serifs should be used, *e.g.*,

A·B·E·F·G·M·P·T·W·

5. Photographs submitted for publication should be printed on glossy paper with somewhat more contrast than that desired in the reproduction.

6. Captions to all figures should be typed in a separate sheet and attached at the end of the paper.

7. The mathematical expressions should be written carefully by hand. Care should be taken to distinguish between capital and small letters and superscripts and subscripts. Repetition of a complex expression should be avoided by representing it by a symbol. Greek letters and unusual symbols should be identified in the margin. Fractional exponents should be used instead of root signs.

NOTICE

No claims will be allowed for copies of journal lost in the mail or otherwise unless such claims are received within 4 months of the date of issue.

6

VARIOUS APPROXIMATIONS FOR THE ISOTOPIC THERMAL DIFFUSION FACTOR. I. APPLICATION TO HELIUM ISOTOPES

S. C. SAXENA AND P. A. PARDESHI

CHEMISTRY DIVISION, ATOMIC ENERGY ESTABLISHMENT TROMBAY, BOMBAY, INDIA

(*Received, September* 8, 1960)

ABSTRACT. Various formulae for the isotopic thermal diffusion factor have been reviewed and a new formula has been derived. Numerical calculations have been performed for the particular case of He^3–He^4 in a region where quantum effects are negligible. These calculations establish the relative adequacy of a comparatively simpler formula advanced by us and will be useful to interpret the recent experimental results of Saxena, Kelley and Watson on the thermal diffusion factor as a function of temperature.

1. INTRODUCTION

Knowledge of the thermal diffusion factor for helium isotopes is important, for thermal diffusion has been used by McInteer, Aldrich and Nier (1948) and Schuette, Zucker and Watson (1950) to enrich He^3 despite its extremely low abundance ($1.3\times10^{-4}\%$) in natural helium and still lower abundance for well helium. Measurements of the isotopic thermal diffusion factor, α_T, as a function of temperature are also important to investigate the intermolecular forces. Moran and Watson (1958) measured the thermal diffusion factor for He^3–He^4 in the temperature range 233°K to 571°K by using an elegant apparatus "Trennschaukel" introduced by Clusius and Huber (1955). Recently Saxena, Kelley and Watson (1960) have extended these measurements to still lower temperatures. These measurements show a much steeper temperature dependence for α_T than given by the existing theoretical expressions. Approximate quantum mechanical calculations of α_T by Saxena (1960) reveal that the quantum corrections are negligible even at the lowest temperature (233°K). Thermal diffusion factor like other transport properties, emerges from the theory as the ratio of infinite determinants, Chapman-Cowling (1953). There are two alternative procedures developed separately by Chapman and Cowling (1953) and by Kihara (1949) to expand these infinite determinants into infinite convergent series. The use of varying number of terms of these series lead to the various approximations on the two schemes. As Moran and Watson (1958) compared their experimental results only with an approximate formula, valid more rigorously for a mixture of heavy isotopes, it would be interesting to explore the possibility of this anomaly

in the use of an inadequate theoretical expression. The purpose of the present paper is to evaluate α_T for He^3–He^4 according to the expressions derived on the two approximation schemes. This will establish the relative usefulness and limitations of the various formulae. A new formula has been derived on the Kihara approximation scheme, taking into consideration terms containing upto the second power of the reduced mass.

2. GENERAL FORMULAE FOR THE ISOTOPIC THERMAL DIFFUSION FACTOR

The Chapman-Enskog kinetic theory of gases expresses the m-th Chapman-Cowling approximation for α_T as follows:

$$[\alpha_T]_m = \frac{5}{2}[X_1X_2A_{00}^{(m)}]^{-1}\left[X_1A_{01}^{(m)}\left(\frac{M_1+M_2}{2M_1}\right)^{\frac{1}{2}}+X_2A_{0-1}^{(m)}\left(\frac{M_1+M_2}{2M_2}\right)^{\frac{1}{2}}\right]. \quad (1)$$

Here X_1 and X_2 are the mole fractions of the two components of molecular weights M_1 and M_2 respectively. The quantity $A^{(m)}$ represents a determinant of $(2m+1)$ order, the general term of which is a_{ij} where i and j range from $-m$ to $+m$ including zero. The minor of $A^{(m)}$ obtained by deleting the row and column containing a_{ij}, is denoted by the symbol $A_{ij}^{(m)}$. To the first approximation, Eq.(1) can be written into the following convenient form:

$$[\alpha_T]_1 = \frac{(6C^*-5)(X_1S_1-X_2S_2)}{X_1^2Q_1+X_2^2Q_2+X_1X_2Q_{12}}, \quad \ldots (2)$$

where

$$S_1 = \left[\frac{M_1}{M_2}\left(\frac{2M_2}{M_1+M_2}\right)^{\frac{1}{2}}A^* - \frac{4M_1M_2A^*}{(M_1+M_2)^2} - \frac{15M_2(M_2-M_1)}{2(M_1+M_2)^2}\right],$$

$$Q_1 = \left[\frac{2}{M_2(M_1+M_2)}\left(\frac{2M_2}{M_1+M_2}\right)^{\frac{1}{2}}A^*\left\{\left(\frac{5}{2}-\frac{6}{5}B^*\right)M_1^2+3M_2^2+\frac{8}{5}M_1M_2A^*\right\}\right],$$

and

$$Q_{12} = \left[15\left(\frac{M_1-M_2}{M_1+M_2}\right)^2\left(\frac{5}{2}-\frac{6}{5}B^*\right)+\frac{4M_1M_2A^*}{(M_1+M_2)^2}\left(11-\frac{12}{5}B^*\right)\right.$$
$$\left.+\frac{8}{5}\frac{(M_1+M_2)}{(M_1M_2)^{\frac{1}{2}}}A^{*2}\right].$$

The expressions for S_2 and Q_2 are obtained from those of S_1 and Q_1 by an interchange of the subscripts for the molecular masses. Here the functions $\Omega^{(b,n)*}$ are the reduced Chapman-Cowling collision integrals and the functions A^*, B^* and C^* are ratios of $\Omega^{(b,n)*}$ and have been tabulated by Hirschfelder, Curtiss and Bird (1954) as a function of the reduced temperature. Second and higher

approximations are conveniently left in the determinant form of Eq. (1) for computational purposes.

For the case of heavy isotopes where the reduced mass, $\frac{M_1-M_2}{M_1+M_2}$, is small, Eq. (1) can be expanded in the powers of the reduced mass. Retaining terms only up to the first power of the reduced mass, one obtains;

$$[\alpha_T]_m = [\alpha_0]_m \left(\frac{M_1-M_2}{M_1+M_2}\right), \qquad \ldots (3)$$

where $[\alpha_0]_m$ is dimensionless thermal diffusion factor and has been given by Mason (1954, 1957a) for $m = 1, 2$ and 3. For $m = 1$, α_0 is given by

$$[\alpha_0]_1 = \frac{15(6C^* - 5)(2A^* + 5)}{2A^*(16A^* - 12B^* + 55)}. \qquad \ldots (4)$$

Expressions for m equal to 2 and 3 are rather lengthy and will not be repeated here.

Eq. (2) transforms into the following form for the case of heavy isotopes when one retains terms up to the second power of the reduced mass, M, (Chapman, 1941):

$$[\alpha_0]_1' = [\alpha_0]_1[1 - \gamma M(X_1 - X_2)], \qquad \ldots (5)$$

where

$$\gamma = \frac{3(5 - A^*)}{2(5 + 2A^*)} - \frac{2(12B^* + 5)}{(16A^* - 12B^* + 55)}.$$

It is interesting to note that $[\alpha_0]'_1$ is now dependent on the relative proportions of the two isotopes unlike Eq. (4).

Kihara (1949) developed an alternative scheme to expand these infinite determinants into convergent infinite series. This procedure is mathematically less straightforward than that of Chapman-Cowling but it has a more physical basis and gives simpler expressions at least in the earlier approximations. Recently, Mason (1957a)has elaborated and extended this procedure and has given the expression upto the second approximation for the thermal diffusion factor. The general formula for the m-th approximation to the thermal diffusion factor on Kihara scheme remains the same as given by Eq. (1) except that now a_{ij} have different meaning. The first approximation $[\alpha'_T]_1$ is again given by Eq. (2) except that the Q's are now defined as follows:

$$Q_1' = \left[\frac{2}{M_2(M_1+M_2)}\left(\frac{2M_2}{M_1+M_2}\right)^{\frac{1}{2}} A^*\left\{M_1^2 + 3M_2^2 + \frac{8}{5}M_1M_2A^*\right\}\right],$$

and

$$Q_{12}' = \left[15\left(\frac{M_1-M_2}{M_1+M_2}\right)^2 + \frac{32M_1M_2A^*}{(M_1+M_2)^2} + \frac{8}{5}\frac{M_1+M_2}{(M_1M_2)^{\frac{1}{2}}}A^{*2}\right] \quad \ldots \quad (6)$$

Using the extended Kihara scheme, Mason (1957a) gave the following formula for the second approximation to α_T:

$$[\alpha'_T]_2 = [\alpha_T]_1(1 + K'_1) + K_2', \quad \ldots \quad (7)$$

where

$$K_1' = h_3h_5 + h_4h_{-6} + h_{-3}h_{-5} + h_{-4}h_6\,, \quad \ldots \quad (8)$$

and

$$K_2' = \frac{5}{2X_1}\left(\frac{M_1+M_2}{2M_2}\right)^{\frac{1}{2}}(h_{-1}h_{-5} + h_1h_6 - h_2h_4 + h_{-2}h_3)$$

$$- \frac{5}{2X_2}\left(\frac{M_1+M_2}{2M_1}\right)^{\frac{1}{2}}(h_1h_5 + h_{-1}h_{-6} - h_{-2}h_{-4} + h_2h_{-3}). \quad \ldots \quad (9)$$

In Eq. (7), $[\alpha_T]_1$ is given by Eq. (2) and the various h_K are similar to those given by Mason (1957a) except that the subscripts characterising the molecular species are all the same.

For the case heavy isotopes, α'_T can again be put in the form of Eq. (3), where $[\alpha_0']_1$ is now given by the following simpler form:

$$[\alpha_0']_1 = \frac{15(6C^*-5)}{16A^*}\,. \quad \ldots \quad (10)$$

The second approximation $[\alpha_0']_2$ can be written in the following form:

$$[\alpha_0']_2 = [\alpha_0]_1(1 + K_0'). \quad \ldots \quad (11)$$

Here $[\alpha_0]_1$ is given by the Eq. (4) and K_0' is a correction factor given by Mason (1957a).

Using Kihara's scheme for approximating transport coefficients, we have worked out the following first approximation to the thermal diffusion factor for a mixture of heavy isotopes in which terms containing upto the second power of the reduced mass have been retained:

$$[\alpha_0']_1' = [\alpha'_0]_1\left\{1 - \frac{(5-3A^*)}{2(2A^*+5)}M(X_1-X_2)\right\}. \quad \ldots \quad (12)$$

This formula is slightly simpler than the one given by Eq. (5) and as shown in the next section, is very useful for the accurate evaluation of α_T of isotopic mixtures

where M is not quite small. Such isotopic mixtures are the mixtures of helium and hydrogen isotopes.

3. CALCULATION OF THE THERMAL DIFFUSION FACTOR FOR HELIUM

Detailed calculations for the thermal diffusion factor of helium have been performed on both the approximation schemes, according to the various formulae discussed in the previous section. The results of this calculation are tabulated in Table I and refer to the following $L-J(12-6)$ law for intermolecular force:

$$E(r) = 4\epsilon \left[\left(\frac{\sigma}{r} \right)^{12} - \left(\frac{\sigma}{r} \right)^{6} \right]. \qquad \ldots \quad (13)$$

Here $E(r)$ is the potential energy of the two molecules at a separation distance r and σ is the molecular separation for which the interaction energy is zero. ϵ is the value of the maximum negative potential energy. The various collision integrals required for these calculations are tabulated by Hirschfelder, Curtiss and Bird (1954).* In those calculations of Table I where the system has been treated as a binary mixture of He^3 and He^4, we have chosen arbitrarily the concentration of He^3 as 5%, a value close to the one used in the work of Moran and Watson (1958). Further, these calculations were performed on a desk calculator and have been subjected to only spot-checking.

TABLE I

Calculated values of the isotopic thermal diffusion factor for Helium

Chapman-Cowling approximation scheme					Kihara approximation scheme				
T^*	$[\alpha_T]_1^{mix}$	$[\alpha_T]_1^{iso}$	$[\alpha_T]'_1{}^{iso}$	$[\alpha_T]_2^{mix}$	$[\alpha_T']_1^{mix}$	$[\alpha_T']_1^{iso}$	$[\alpha_T']_1{}'^{iso}$	$[\alpha_T']_2^{mix}$	$[\alpha_T']_2^{iso}$
5	0.0671	0.0695	0.0677	0.0690	0.0702	0.0718	0.0707	0.0694	0.0716
7	0.0724	0.0751	0.0732	0.0747	0.0742	0.0759	0.0747	0.0755	0.0779
9	0.0744	0.0788	0.0753	0.0760	0.0779	0.0797	0.0785	0.0778	0.0803
20	0.0767	0.0794	0.0774	0.0803	0.0802	0.0820	0.0808	0.0809	0.0832
40	0.0768	0.0794	0.0774	0.0801	0.0802	0.0820	0.0808	0.0808	0.0832
60	0.0764	0.0791	0.0771	0.0799	0.0799	0.0816	0.0805	0.0804	0.0827
80	0.0763	0.0789	0.0769	0.0796	0.0797	0.0814	0.0803	0.0805	0.0826
100	0.0761	0.0787	0.0767	0.0794	0.0795	0.0812	0.0800	0.0800	0.0829
200	0.757	0.0781	0.0762	0.0784	0.0790	0.0806	0.0795	0.0797	—

*It may be pointed out that there is a misprint in the value of the collision integral $\Omega^{(1,1)*}$ for $T^* = 100$. It should read as 0.5170 instead 0.5130.

In columns 2, 3, 4 and 5 of Table I are recorded the values of the different approximations to α_T as a function of the reduced temperature ($T^* = kT/\epsilon$) according to Chapman-Cowling scheme; while the columns 6, 7, 8, 9 and 10 report the results on Kihara scheme. Values of α_T listed in columns 2 and 3 of Table I have been obtained according to the Eqs. (2) and (4) respectively. The two sets of values differ appreciably and reveal the fact that for Helium, terms involving only first power of the reduced mass are not enough ; a result previously pointed out by Winter (1950). It is, therefore, interesting to consider terms involving still higher powers of M. Chapman (1941) derived an expression, Eq. (5), which takes into account the terms upto the second power of M. Calculated values according to this formula are given in column 4 of Table I. It will be seen that these values are appreciably different ($\simeq 2.4\%$) from $[\alpha_T]_1^{iso}$ but are in good agreement with the $[\alpha_T]_1^{mix}$ values ($\simeq 0.9\%$). Values of $[\alpha_T]_2$ computed according to Eq. (1) with $m = 2$ are shown in column 5. These values are approximately 4% higher than the $[\alpha_T]_1^{mix}$ values, establishing thereby that the convergence of the series is fast enough and the error involved, because of the neglect of the third and higher approximations, is small. This inference is very welcoming in view of the fact that the higher approximations will involve evaluation of seven and higher order determinants and can be safely avoided till we considerably improve the precision and accuracy of the measurements. It is also very interesting to note that $[\alpha_T]'^{iso}_1$ values are in better agreement with the $[\alpha_T]_2^{mix}$ values than the $[\alpha_T]_1^{mix}$ values. The authors therefore feel that the simple formula for α_T as given by Eq. (5) is preferable to the complicated form of Eq. (2) and still more compli- cated form as given by Eq. (1).

Results obtained using similar approximations, but on Kihara scheme are listed in columns 6, 7, 8 and 9, and are seen to follow the same qualitative trend. In column 10 are tabulated for comparison the results obtained from a formula which considers terms upto the second approximation but retains only the first power of reduced mass, Saxena and Mason (1958). These values of $[\alpha'_T]_2^{iso}$ are systematically higher than the $[\alpha'_T]_2^{mix}$ values. As the convergence for the Kihara approximation scheme is still faster than that of Chapman-Cowling, we are of the opinion that the neglect of the second power of the reduced mass is much more serious. A critical examination of all the values obtained on Kihara approximation scheme again leads to the same conclusion that the values obtained by using the simpler formula, Eq. (12), which considers terms upto the second power of reduced mass, is preferable to the rest of all, both for accuracy and simplicity.

A critical examination of the various approximations for α_T on the two approximation schemes for realistic intermolecular potentials and for a few mathematically simple systems, was done by Mason (1957a and 1957b). Mason (1957b) considered three types of mixtures viz. (1) Lorentzian, (2) Quasi-Lorentzian and (3) Heavy isotopic mixtures. Unfortunately our system is not identical to any of these

but resembles to (3) in as much as all the interactions are identical but the two masses differ considerably. Our numerical calculations of Table I reveal that Kihara approximation scheme is preferable to Chapman-Cowling and is in conformity with the conclusions of Mason (1957b) for mixtures of heavy isotopes.

4. CONCLUSIONS

Our numerical calculations for $\varkappa_T$ of helium isotopes establish that Kihara approximation procedure is better than that of Chapman and Cowling. With He^3 present in trace, a simple formula derived, treating the mixture of He^3 and He^4 as a heavy isotopic mixture but retaining terms upto the second power of the reduced mass, will yield results within the range of experimental error. This formula is also preferable in view of comparative simplicity and accuracy.

ACKNOWLEDGMENT

The authors are thankful to Dr. J. Shankar for his kind interest and making available to us all the facilities.

REFERENCES

Chapman, S., 1941, *Proc. Roy. Soc.*, **A177**, 38.

Chapman, S. and Cowling, T. G., 1953, The Mathematical Theory of Non-Uniform gases, Cambridge University Press, England.

Clusius, K. and Huber, M., 1955, *Z. Naturforsch.*, **10A**, 230.

Hirschfelder, J. O., Curtiss, C. F., and Bird, R. B., 1954, The Molecular Theory of Gases and Liquids, John Willey & Sons, Inc., New York.

Kihara, T., 1949, Imperfect Gases, originally published in Japanese (Asakusa Book Store, Tokyo) and translated into English by the U.S. office of Air Research, Wright-Patterson Air Force Base, Chap. 6; see also 1953, *Revs. Modern Phys.*, **25**, 831.

Mason, E. A., 1954, *J. Chem. Phys.*, **22**, 169.

Mason, E. A., 1957a, *J. Chem. Phys.*, **27**, 75.

Mason, E. A., 1957b, *J. Chem. Phys.*, **27**, 782.

McInteer, B. B., Aldrich, L. T., and Nier, A. O., 1948, *Phys. Rev.*, **74**, 946.

Moran, T. I., and Watson, W. W., 1958, *Phys. Rev.*, **109**, 1184.

Saxena, S. C., 1960, unpublished calculations.

Saxena, S. C., Kelley, T. G. and Watson, W. W., 1960, In course of publication.

Saxena, S. C., and Mason, E. A., 1958, *J. Chem. Phys.*, **28**, 623.

Schuette, O. F., Zucker, A. and Watson, W. W., 1950, *Rev. Sci. Instr.*, **21**, 1016.

Winter, E. R. S., 1950, *Trans Faraday Soc.*, **46**, 81.

7

X-RAY THERMAL DIFFUSE SCATTERING IN AZELAIC AND PIMELIC ACIDS*

R. L. BANERJEE, M. L. CANUT AND J. L. AMOROS

Sección de Termodinámica Cristalina

DEPARTAMENTO DE CRISTALOGRAFIA. C.S.I.C. MADRID

(*Received, November* 9, 1960)

Plate II

ABSTRACT. Thermal diffuse scattering of azelaic and pimelic acids is studied by X-ray diffraction methods and compared with the observed diffuse scattering in other dycarboxilic acids. The interpretation of such diffuse scattering is done both by considering the propagation of thermal elastic waves accordingly with the crystal structure and by using the difference Fourier transform approach which gives account of the extended continuous regions of diffuse scattering. Also, the dynamic symmetry of the crystals is studied as deduced from the consideration of the observed diffuse scattering.

The study of X-ray thermal diffuse scattering is interesting because it gives the unique insight of the dynamics of the crystal. The treatment of this problem is complicated and the thermal wave theory is perhaps the best approach to the question in simple (ionic) crystals. In molecular crystals, however, where there is evidently a far complicated atomic pattern, the problem can be reduced greatly by considering the fact that the molecules can be treated as rigid bodies and therefore most of its dynamical picture is given by the movement of big structural units, the molecules. A long term programme of research was developed in the Departamento de Cristalografia, Madrid, with the aim of elucidating the status of the molecular crystals. Many types of such crystals were studied (hexamine Canut and Amorós, 1958), pentaerythritol (Alonso *et al.*, 1958), naphthalene (Acha *et al.*, 1958), anthracene (Annaka and Amorós, 1960, etc.) and a general theory was given to explain the continuous thermal diffuse scattering discovered in such crystals (Amorós *et al.*, 1960). It is therefore of interest to check the theory in another group of molecular crystals for which no previous computations were made. The group of molecular substances chosen is that of the dicarboxylic acids with odd number of carbon atoms.

The interest of the present research lies in the fact that the dicarboxylic acids with even number of carbon atoms have already been studied (Canut and

*This research was in part supported by the Directorate of Solid-State Sciences, Air Force Office of Scientific Research, through the European Office of Air Research and Development Command, under Contract AF 61(052)—193.

Amorós, 1957) and therefore a direct comparison of the two groups can easily be done and thereby a general picture of the lattice dynamics of long chain compounds can be drawn.

ANTECEDENTS

The structure of pimelic acid COOH-$(CH_2)_5$-COOH has been determined by MacGillavry and his coworkers (1948). The crystal belongs to the monoclinic system and space group I $2/a$ and contains four molecules per unit cell.

The unit cell dimensions are :

$$a = 9.84\text{Å}, \quad b = 4.89\text{Å}, \quad c = 22.43\text{Å} \quad \text{and} \quad \beta = 130° 46'$$

The crystal structure of azelaic acid COOH-$(CH_2)_7$-COOH has not been determined as yet. According to Caspari (1928) the crystal belongs to the monoclinic system and contains four molecules per unit cell.

The unit cell dimensions are :

$$a = 9.72\text{Å}, \quad b = 4.83\text{Å}, \quad c = 27.14\text{Å} \quad \text{and} \quad \beta = 129°30'$$

The space group of azelaic acid has not been determined, but a careful observation of the distribution of the diffuse scattering of azelaic acid studied in the present work reveals that the distribution of the diffuse maxima obeys the same extinction condition as those of pimelic acid, i.e., $h+k+l$ = even. Therefore, the space group of azelaic acid should be the same as that of pimelic acid, i.e., I $2/a$, and the crystal structures of the two acids should also be the same, except for the difference in length of the molecules.

While obtaining azelaic acid crystals at room temperature from a slightly warm acetone solution, we happened to obtain azelaic acid crystals of another modification stable at room temperature. Much earlier Caspari (1929) obtained a high temperature modification of azelaic acid by slowly cooling down a hot solution of the acid.

Later, Dupré La Tour (1935) obtained this modification by slowly cooling down the azelaic acid melt.

The lattice constants of the modification that we have obtained along with those of the modification obtained by Caspari are given below:

	a	b	c	β
Azelaic acid (II)	5.69 Å	9.57 Å	27.78 Å	136°39′
α-azelaic acid (9)	5.61 Å	9.58 Å	25.35 Å	136°10′

EXPERIMENTAL METHOD

Single crystals were obtained from an acetone solution. The crystal used in the experiment had the dimensions of about $1.5 \times 1.0 \times 1.0$ mm^3. It was

mounted with its [010] axis vertical and considering its monoclinic symmetry, Laue photographs were taken at each 5° of a zone of 180°. Ilford industrial *G* films, filtered Cu $k\alpha$ radiation at 40KV., 20mA, and a Unicam camera with cillindrical film holder was used. The exposure time was 2 hours. In order to register the thermal diffuse scattering on the reciprocal lattice level $[010]_n$, the reciprocal co-ordinates ζ and ξ were measured for each diffuse spot with the help of the Bernal Chart after substracting the size of the corresponding Laue spot to correct for the crystal size and the divergence of the x-ray beam effects. We plotted the diffuse reflections on each reciprocal lattice level by using transparent paper and Martin's Chart (1956). This method saves much time in the tedious task of passing the photographic record of the diffuse scattering to the diffraction space (i.e. the reciprocal space). The crystal, x-ray beam orientation becomes unequivocally fixed when the diffuse scattering domains of each level of the reciprocal lattice are compared with the corresponding reciprocal lattice net, due to the fact that the thermal diffuse scattering maxima are always to be on the reciprocal lattice points.

Diffuse scattering domains in $[010]_n$ *of azelaic acid*

Laue patterns of dicarboxylic acids show two types of diffuse spots:

a) Streaks, characteristic of the molecules in chains, extended between the reciprocal lattice points when plotted in it.

b) Independent, round and definite spots, some of them very strong, giving a diffuse cloud around non-forbidden reciprocal lattice points.

With the [010] mounting of the crystals, the streaks always appear in the photograph cutting the equator at right angles and extending across the higher levels (Fig. 1, Plate II).

$[010]_0$ *level* :

The diffuse domains of this level are shown in the Fig. 2. The strongest round diffuse spot is associated with the reciprocal lattice point 200. The planes corresponding to this point contain the layers of the chains. Other round spots appear at the reciprocal lattice points with $h = 2n$ and $l = 2n$, that is, at the non-forbidden ones. The most prominent of them being those associated with 200, $40\bar{2}$, $60\bar{2}$, $\bar{4}08$, $\bar{4}010$, $\bar{4}022$, $\bar{6}012$, $\bar{6}010$, lattice points. Continuous diffuse scattering domains appear in the rows of the reciprocal lattice points having $l = \text{const} = \text{even}$.

The strongest continuous domains are extended along the rows with

$$l = 10,\ 18,\ 20,\ 22,\ 23$$

$[010]_1$ *level* :

The round diffuse spots of this level (Fig. 3) follow the extinction condition $h+l = \text{odd}$.

Indian Journal of Physics, Vol. 35, No. 2

Fig. 1. Laue photograph. Azelaic acid. Vertical axis [010].

The streaks of this level unlike those of the zero level, do not appear in the very well defined continuous zones of $l = \text{const.}$

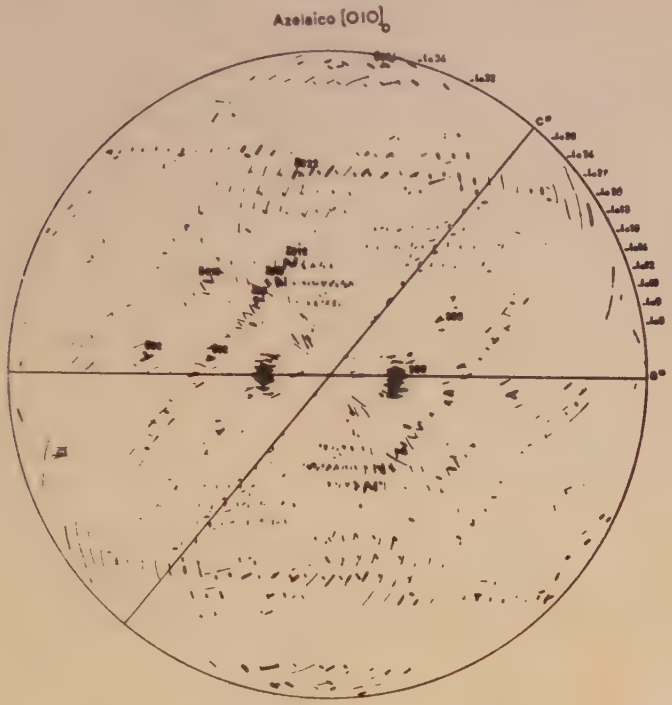

Fig. 2. Azelaic acid. Diffuse domains in $[010]_0$.

The strongest diffuse spots are associated with the following reciprocal lattice points: 110, 21$\bar{1}$, 011, 310, 11$\bar{8}$, 111$\bar{0}$, 11$\bar{6}$, 21$\bar{2}\bar{1}$.

$[010]_{\frac{1}{2}}$ *level*:

The plotting of the diffuse reflections in this inter-layer (Fig. 4) was done only for those which extend across the zero and the first levels.

Moderately strong continuous domains of diffuse scattering appear in this level extended along the rows of the reciprocal lattice points having $l = 10, 22, 32$.

Apart from this there appears a strong diffuse domain at $2\ \frac{1}{2}\ 0$ which is the section of the very strong round diffuse spot 200 of the zero level.

THREE DIMENSIONAL ANALYSIS OF THE DIFFUSE SCATTERING

From the analysis of the domains of the continuous diffuse scattering, it is clear that these domains, which appear along the rows of reciprocal lattice points with $l = \text{const}$, that is, perpendicular to the chain direction (c axis), in all the levels $[010]_0$, $[010]_{\frac{1}{2}}$ and $[010]_1$, are actually sheets perpendicular to c axis of the crystal

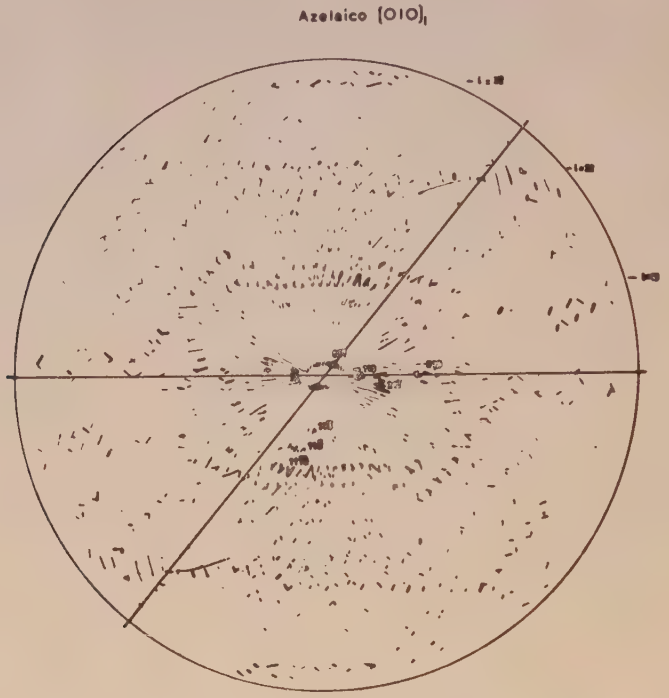

Fig. 3. Azelaic acid. Diffuse domains in $[010]_1$.

Fig. 4. Azelaic acid. Diffuse domains in $[010]_{\frac{1}{2}}$.

in three dimensions. The sheets passing through the reciprocal lattice planes with $l = 10$, 22 and 32 are the most prominent ones. These sheets are confined within a zone of 90° about the chain direction extending 45° on either side of it.

COMPARISON BETWEEN THERMAL DIFFUSE SCATTERING OF AZELAIC AND PIMELIC ACIDS

The morphology of the thermal diffuse scattering of pimelic acid has previously been studied by Canut and Amorós (1957). Fig. 5 shows the diffuse scattering domains of pimelic acid in the $[010]_0$ level.

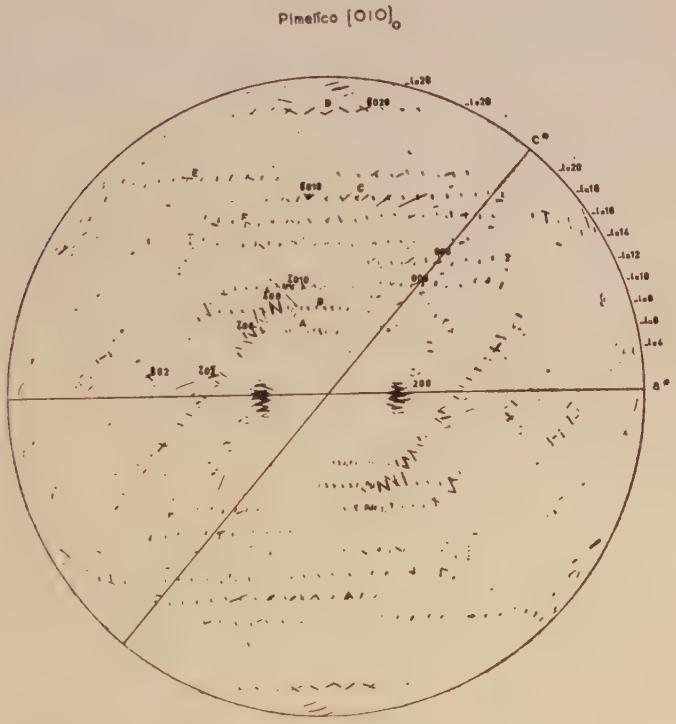

Fig. 5. Pimelic acid. Diffuse domains in $[010]_0$.

Comparison of the diffuse scattering domains of azelaic acid in $[010]_0$ level (Fig. 2) with that of pimelic acid (Fig. 5) reveals the fact these two acids, belonging to the odd series of dicarboxylic acids, give extremely similar diffuse scattering patterns. The only difference is that whereas in pimelic acid the strongest continuous diffuse scattering domains appear extended along the reciprocal lattice planes having $l = \text{const} = 6, 8, 10$, etc., those of azelaic acid appear in the planes having $l = \text{const} = 10, 18, 20, 22$ and 32.

But this is only an apparent difference. In fact the spatial distribution of these domains is the same in both the cases. The differences in the values of l are due to the fact that the lattice constants of the two acids are different.

INTERPRETATION

The interpretation of the diffuse scattering of pimelic and azelaic acids will be done together in order to have a correlated idea about the dynamics of the odd-dycarboxylic acids, and to be able to relate the results of this series with those of the even-series already studied in this laboratory.

PROPAGATION OF WAVES

It is well known that thermal waves in the crystals affect the form and extension of the diffuse scattering domains in the reciprocal space. This has been shown by Londsdale (1948) and others.

The theory of crystal dynamics shows that the diffuse scattering domains always extend in the reciprocal space in the direction of the propagation of the waves, either longitudinal or transverse.

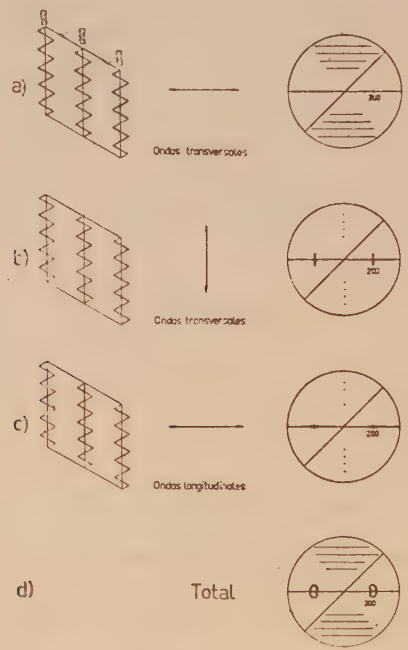

Fig. 6. Scheme of the effect of wave propagation in reciprocal space of a chain-like crystal.
a) Transverse waves travelling at right angles to the chains.
b) Transverse waves travelling along the chains.
c) Longitudinal waves travelling at right angles to the chains.
d) Total effect.

Fig. 6 (Amorós and Canut, 1958) shows the effects of different types of wave on the distribution of diffuse scattering in the reciprocal lattice. Thus

Fig. 6 (a) shows the effect of the transverse waves propagating perpendicular to the chain direction which affect the relative chain-chain positions but not those of the atoms within the chains, in the distribution of diffuse scattering in the reciprocal lattice level $[010]_0$. Figs. 6 (b) and 6 (c) show the effects of transverse waves which propagate parallel to the chains affecting the relative positions of the atoms in the chains, and longitudinal waves which propagate perpendicular to the chains affecting the chain-chain interspace, respectively in the same reciprocal lattice level. Fig. 6 (d) shows the combined effect of the three types of waves mentioned above, on the form of the diffuse scattering domains in the said reciprocal lattice level.

The effect of the longitudinal waves in the direction of the chain has not been observed in either cases of the dicarboxylic acids studied.

In the dicarboxylic acids the molecular chains are parallel to [001] axis of the crystal therefore, the streaks that we have observed in the Laue photographs and are represented by the diffuse domains extended at right angles to the chain direction in the reciprocal lattice, are due to the waves of the first kind, i.e., the transverse vibrations of the chains propagating in the direction perpendicular to them. This we suppose to be the most important movement in these acids. As this kind of movement does not affect the relative positions of the atoms within the chain it is not easily detectable by normal structural method.

The second and the third kind of waves mentioned above determine the form of the diffuse domain around the reciprocal lattice point 200. This is the second feature of these crystals and is explicable with the help of the Figs. 6(b) and 6(c).

EXTENDED CONTINUOUS DOMAINS OF DIFFUSE SCATTERING

As we have stated above, the effect of the transverse wave propagating perpendicular to the chain direction on the shape of the diffuse scattering domains is to make them elongated along the direction perpendicular to that of the chain. Fig. 6(a) schematically represents this effect. While this figure explains the presence of the continuous domains of diffuse scattering extended along the rows of reciprocal lattice points having l = constant, it does not say anything about the extent of the elongation of these domains. On the other hand, the presence of continuous diffuse scattering regions has been observed in the cases of hexamine, anthracene, pentaerythritol, naphthalene, etc, studied in this laboratory, where the presence of the kind of transverse wave represented by fig. 6(a) might not be very important.

Moreover this kind of diffuse scattering is more clearly observed in a zone of 90° about the chain direction extending 45° on either side of it and these diffuse domains extend even across the forbidden reciprocal lattice points.

Therefore in order to explain this kind of diffuse scattering we have undertaken the "difference Fourier transform" (DFT) approach (Amorós *et al*; 1960) which assumes the presence of independent molecular vibrations in the crystal. The theory of this approach is given in the following paragraph.

DIFFERENCE FOURIER TRANSFORM

The Fourier transform of a molecule "at rest" is given by

$$G_R = \sum_{n=1}^{N} f_n \exp\,(2\pi i\, \bar{r}_n.\, \bar{S}), \qquad \ldots \quad (1)$$

where f_n is the atomic scattering factor without temperature correction. The effect of a harmonic movement in the molecule is the correction of the atomic scattering factor by the well known Debye factor,

$$f \exp\,(-M). \qquad \ldots \quad (2)$$

The Fourier transform of a molecule under thermal agitation is given by

$$G_T = \sum_{n=1}^{N} f_n \exp\,(-M) \exp\,(2\pi i\, \bar{r}_n.\, \bar{S}). \qquad \ldots \quad (3)$$

Since the molecular Fourier transform is the scattered radiation of the molecule, the difference

$$G_R - G_T \qquad \ldots \quad (4)$$

corresponds to the modification of the scattering space by the thermal motion of the molecule.

Thermal diffuse scattering is due to the x-ray diffraction of crystals under thermal agitation. Therefore relation (4) can be a direct clue to the interpretation of such diffuse scattering. In order to compare directly the observed values of the thermal diffuse scattering (intensities) with the molecular-transform functions, we must multiply G by its complex conjugate $G*$.

A general way to compute molecular Fourier transforms is to use

$$G = \Sigma\, f_n \exp\, 2\pi i\, (hx_n + ky_n + lz_n) \qquad \ldots \quad (5)$$

where h, k, l can be fractional numbers. The expression (5) corresponds to the molecular structure factor at the point (hkl) of reciprocal space. In the case of a unit cell with four molecules, the x-ray scattered intensity of the four independent molecules (neglecting phase relationship) will be given by

$$\sum_{1}^{4} I_j^2 = \sum_{1}^{4} (A_j^2 + B_j^2) \qquad \ldots \quad (6)$$

corresponding to the molecules at rest. When subject to thermal motion, the intensity of the four independent molecules will be given by

$$I_{mot} = \sum_{1}^{4} (A_j^2 + B_j^3)\ 1 - \exp\left(-2B \frac{\sin^2 \theta}{\lambda^2} \right) \quad \ldots \quad (7)$$

and the effect of the independent motion of the 4 molecules will be given by

$$DFT = I_{rest} - I_{mot} = \sum_{1}^{4} (A_j^2 - B_j^2) \left\{ 1 - \exp\left(-2B \frac{\sin^2 \theta}{\lambda^2} \right) \right\} \quad \ldots \quad (8)$$

Expression (8) is just the difference in scattered intensities of the four molecules at rest and at motion. This expression gives in a direct way the effect, in diffraction space of the independent molecular motion in crystals. It has, for simplicity, been named the "difference Fourier transform" (*DFT*) of the molecules.

COMPUTATION OF THE MOLECULAR FOURIER TRANSFORMS OF PIMELIC ACID

For the computation of the molecular transform of pimelic acid we have utilised the atomic co-ordinates given by Mac-Gillavry and others (1948).

Scattering amplitudes for the individual molecules are calculated and hence we have got the difference of the intensities of scattering ($I_{rest} - I_{mot}$) by the individual molecules at rest and on vibration, by multiplying the squares of the scattering amplitudes by a factor $1 - \exp(-2B \sin^2\theta/\lambda^2)$, where B is the temperature factor. In our case of pimelic acid, owing to the unavailability of the value of B, we have used $B = 2\text{A}^2$. This value of B has been found to be that for succinic acid in the direction of the carbon chain. But as we are making the calculation of a limited zone of the reciprocal lattice about the direction of the chain, where the effect of the independent movement is more important, we have adopted this value of B (i.e. $B = 2$) as an approximate one for pimelic acid.

Because of the two-fold axis of symmetry of the molecules, scattering amplitude corresponding to $h = 2n$ (where n is any integer), comprises of only A and those corresponding to $h = 2n+1$, of only B, where

$$A = \sum_{n} f_n \cos 2\pi(hx + hy + lz)$$

and

$$B = \sum_{n} f_n \sin 2\pi(hx + ky + lz)$$

Now, we have to calculate the $\Sigma(I_{rest} - I_{mot})$ i.e., the DFT for all the four molecules of the unit cell.

But due to the symmetry of the crystal we have the following relations among the A's and B's of the different molecules of the cell:

$$
\begin{aligned}
&B_1 = B_2 = B_3 = B_4 = 0 \quad \text{when } h = 2n \\
&A_1 = A_2 = A_3 = A_4 = 0 \quad \text{when } h = 2n+1 \\
&A_1 = A_3 \text{ when } h = 2n \text{ and } l = 2n \\
&A_1 = -A_3 \text{ when } h = 2n \text{ and } l = 2n+1 \\
&A_1 = A_4 \text{ when } h = 2n \text{ and } l = 2n \\
&A_1 = -A_4 \text{ when } h = 2n \text{ and } l = 2n+1 \\
&B_1 = B_3 \text{ when } h = 2n+1 \text{ and } l = 2n \\
&B_1 = -B_3 \text{ when } h = 2n+1 \text{ and } l = 2n+1 \\
&B_1 = B_4 \text{ when } h = 2n+1 \text{ and } l = 2n \\
&B_1 = -B_4 \text{ when } h = 2n+1 \text{ and } l = 2n+1
\end{aligned}
\qquad (R)
$$

Thus we see that the absolute values of A's and B's for a particular reflection are the same for all the four molecules of the unit cell.

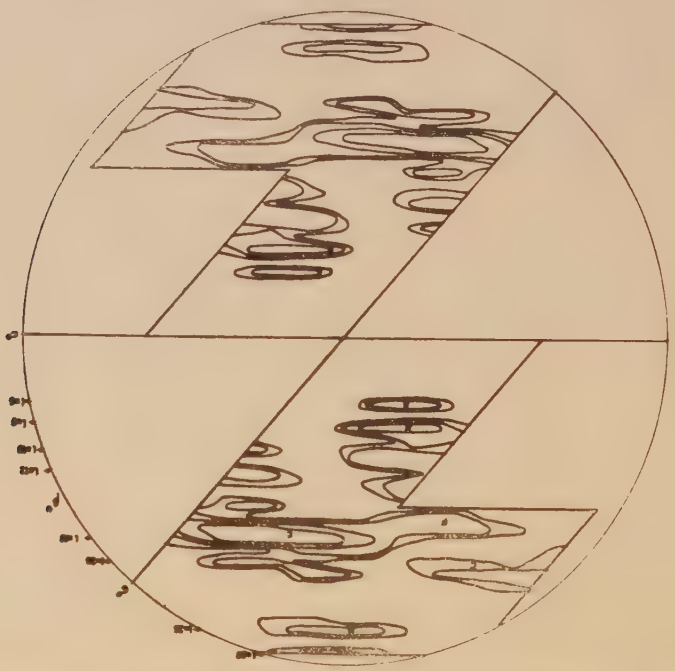

Fig. 7. Pimelic acid. Theoretical isodiffusion lines computed with DFT in the region where the effect of independent motion can be considered.

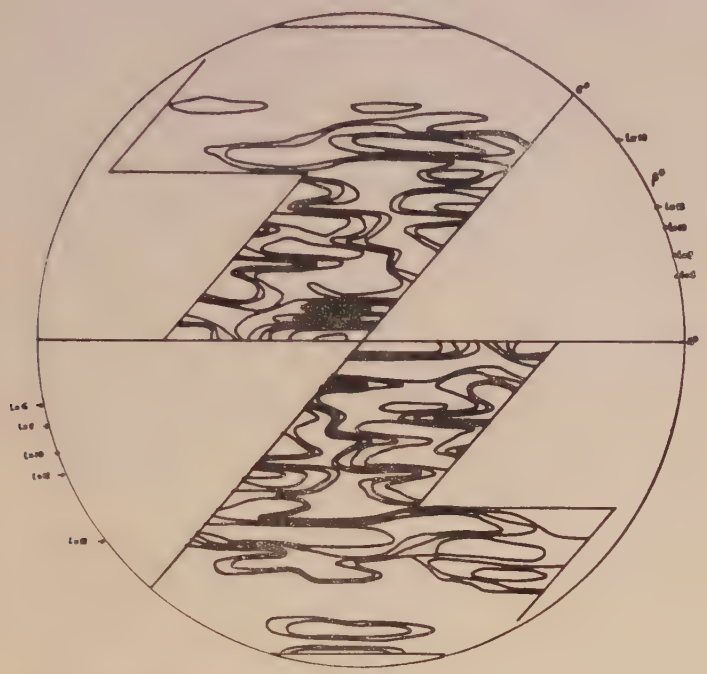

Fig. 8. Pimelic acid. $[010]_0$.
Upper part: Molecular FT_{rest}. Lower part: Molecular FT_{mot}.

Now by definition,

$$DFT = \sum_{1}^{4} (I_{rest} - I_{mot})_j \qquad \text{where } j = 1, 2, 3, 4$$

$$= \sum_{1}^{4} (A_j^2 + B_j^2) \quad \{1 - \exp(-2B \sin^2\theta/\lambda^2)\}$$

where j is the number of molecule of the unit cell.

So, in our case, applying the relations (8), we get

$$DFT = \sum_{1}^{4} (I_{rest} - I_{mot})_j$$

$$= 4A_1^2\{1 - \exp(-2B \sin^2\theta/\lambda^2)\} \quad \text{for } h = 2n$$

and $$= 4B_1^2\{1 - \exp(-2B \sin^2\theta/\lambda^2)\} \quad \text{for } h = 2n+1$$

The difference of intensity $(I_{rest} - I_{mot})$ thus calculated have then been plotted on the reciprocal lattice net and the lines of equal $(I_{rest} - I_{mot})$ values of 20, 35, 70 and 140 have been drawn.

Figs. 5 and 7 are the experimental diffuse scattering pattern and the corresponding DFT map, respectively. The strong continuous diffuse scattering domains

A, B, C and D as also the comparatively weaker ones E and F in Fig. 5 are represented by strong A, B, C, D, and weak E and F of Fig. 7.

The agreement between the experimental and theoretical patterns (Figs. 5 and 7) amply justifies the validity of the DFT approach of interpreting the observed distribution of the extended continuous diffuse scattering and their origin. Fig. 8 shows the molecular Fourier transform maps of the molecules at rest and on motion. Comparison of the Fig. 8 with Fig. 7 shows the superiority of the DFT approach over that of molecular Fourier transform as expected theoretically.

THERMAL MOTION AND CRYSTAL SYMMETRY

We have observed in our present work as also in the previous work in this laboratory that the streaks which appear in the Laue photographs do not always follow the space group extinctions; in the sense that they extend even across the forbidden points of the reciprocal lattice.

This we explain to be due to the fact that the space group symmetry at some instantaneous positions of the molecules of the crystal undergoing thermal vibration (dynamic space group) is different from that of the crystal considered at rest (static space group) (Amorós and Canut, 1960).

Normal methods of structure analysis determine only the static space group. This procedure cannot detect the existence of the dynamic space group because of the fact that the instantaneous change of symmetry due to thermal motion does not change the positions of the Bragg reflections which depend only on the average central positions of the atoms. The thermal motion has got no effect on the Bragg reflections other than diminishing their intensities. Thus, this change of symmetry due to thermal vibrations cannot be detected by normal Fourier methods of Structure analysis.

Fig. 9 shows one complete unit cell containing the molecules in their respective positions and another containing the elements of symmetry corresponding to the space group $I2/a$ of the azelaic acid crystal.

The antiphase vibration represented by the arrow (1) is that due to a transverse wave propagating along the normal to the chain direction. Due to this kind of vibration of the glide plane a, the two fold axes in the centres of the molecules and the centres of symmetry within the hydrogen bonds vanish, giving the space group $P2_{1/n}$ to the crystal at some instantaneous state of the molecules undergoing vibrations.

The symmetry elements that vanish as a result of the vibration represented by the arrow (1) in the Fig. 9 also vanish as a result of that represented by the arrow (3). Therefore, the space group (dynamic) due to the latter kind of vibration is also $P2_{1/n}$.

The arrow (2) represents the antiphase libration of the chains about the axes along their direction. The screw axes lying in between the chains vanish at some instantaneous state of the molecules undergoing libration giving the space group (dynamic) $P_{2/n}$ to the crystal.

The systematic extinctions in $[010]_0$ levelowing to n are the same as those for I and, therefore, the extinction condition $h-l =$ even, in the $[010]_0$ level is maintained.

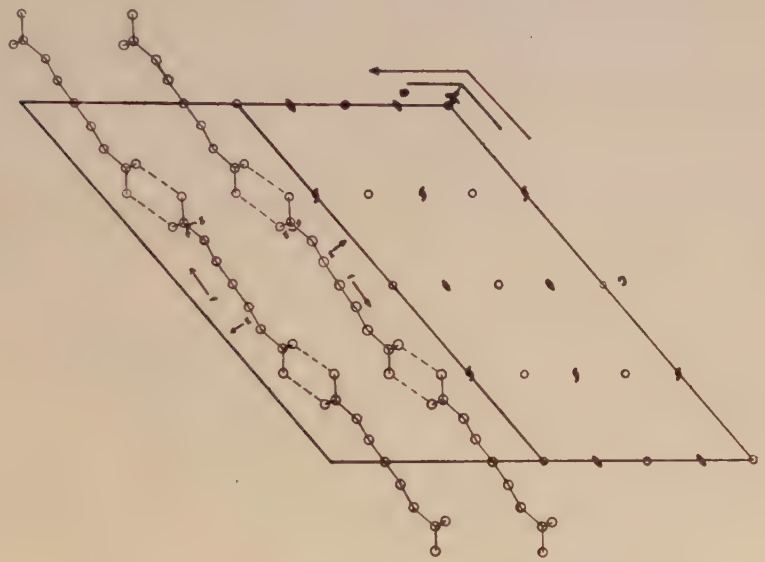

Fig. 9. Pimelic acid. Projection of the structure on (010).

COMPARISON BETWEEN THERMAL DIFFUSE SCATTERING OF THE DICARBOXYLIC ACIDS OF EVEN AND ODD SERIES

The difference between the distributions of the diffuse scattering zones in the reciprocal lattice of the acids belonging to the two series is not very great. The general features of these distributions are essentially the same. In the case of the acids belonging to the even series the extended continuous zones of diffuse scattering appear as well defined, even by spaced sheets perpendicular to the chain direction in the reciprocal space. The spacing of these sheets is reciprocal to 2.5Å. This distance 2.5Å corresponds to the zig-zag distance of the carbon atoms of the molecular chain and the length of the hydrogen bond binding the molecules of the same chain. That means the periodicity in the distribution of the continuous diffuse zones along the direction of the chain in the reciprocal space shows a well marked reciprocal relation to that of the chains. This reciprocal relation

is also clearly exhibited by the DFT maps of the acids of the even series (Amorós and Canut, 1958).

But it is less clearly exhibited by the distribution of the continuous diffuse zones and their DFT representations of the acids of the odd series. A probable reason of the observed difference between the distributions of the continuous diffuse zones of the acids belonging to the two series is that in the case of the even series acids the chains are well defined but those in the case of the odd series are distorted. In the case of even series the carbon atoms of a chain are coplanar and the long axes of the molecules in the same chain are colinear whereas in the case of odd series neither the carbon atoms are coplanar nor the molecular axes are colinear.

REFERENCES

Acha A., Canut M. L. and Amoros, J. L., 1958, *Bol. R. Soc. Esp. Hist. Natt.*, (G) **56**, 405.
Alonso, P., Canut, M. L. and Amoros, J. L., 1958, *Bol. R. Soc. Esp. Hist. Nat.*, **56**, 379.
Annaka, S. and Amoros, J. L., *Z. Kristallog.*, (In press).
Amoros, J. L. and Canut, M. L., 1958, *Bol. R. Soc. Esp. Hist. Nat.*, (G) **56**, 25.
Amoros, J. L. and Canut, M. L., 1958, *Bol. R. Soc. Esp. Hist. Nat.* (G)**56**, 305.
Amoros, J. L., Canut, M. L. and Acha, A., 1960, *Z. Kristallog*, **114**, 39.
Amoros, J. L. and Canut, M. L., 1960, *Bol. R. Cos. Esp. Hist. Nat.*, (G) 57,
Canut, M. L. and Amoros, J. L., 1957, *P. Dep. Crist. Min.*, **3**, 15.
Canut, M. L. and Amoros, J. L., 1957, *P. Dep. Christ. Min.*, **3**, 27.
Canut, M. L. and Amoros, J. L., 1958, *Bul. R. Soc. Esp. Hist. Nat.*, (G) **56**, 323.
Caspari, W. A., 1928, *J. Chem. Soc. London*, **30**, 3235.
Caspari, W. A., 1929, *J. Chem. Soc. London*, **30**, 2709.
Dupre la Tour F., 1935, *Compt. Rendus*, 479.
Lonsdale, K., 1948, Crystals and X-rays, London, Bell, Sons.
Mac Gillavry, C. H., Hoodchagen G. and Sixma, F. L. J., 1948, *Rec. trav. Chem. Pays. Bas.*, **67**, 869.
Martin, W. G., 1956, *J. Appl. Phys.* **27**, 514.

8

INVESTIGATIONS INTO THE LOW ENERGY GAMMA RAY BACKGROUND AND ITS VARIATIONS

BIJON ROY, PROBIR K. SANDELL AND AJOY K. CHOUDHURY

Department of Experimental Medical Sciences,
Institute of Post-graduate Medical Education & Research, Calcutta

(*Received, July* 7, 1960)

ABSTRACT. The gamma-ray background of Calcutta as determined by scintillation spectrometry using a NaI (thallium activated) crystal consists of two broad energy bands being contributed by the radioactive substances present in the soil, air and building materials and identified as those from the radium and thorium family. The background so determined indicates that there are two possible regions of low level counting which is achieved by choosing an optimum channel level and channel width. The variation in intensity of the background is restricted mostly to lower energy region of the background spectrum and is under further investigation.

INTRODUCTION

In low level counting using scintillation counters the background count is always a limiting factor. On the other hand in certain low level counting, as in bio-medical tracer technique different authorities, (Johnston, 1955; Anderson and Libby, 1957) Medical Research Council (Report 1956) have stressed the need of low doses of radioactive tracers in diagnostic and investigative works. Possibly it is safe to use a dose which is of the order of the natural background in its activity. Furthermore, in *in vivo* measurements during bio-medical tracer works, an effective shielding against the background is often not possible. Thus, in all the above cases an attempt at low level scintillation counting must essentially be preceded by a survey of the nature of the background at the particular place. This means the determining of the energy distribution in the background spectrum, the position of its main peaks, if any, and their relative intensities. As the gamma-emitters usually used in low level counting as in bio-medical work, like I (131), Fe (55), Cr (51), Au (198) etc., have characteristic energies below 700 KeV it is of interest to analyse spectrometrically the region below this.

Recently, many excellent review works on low level counting have been published (Hayes, Anderson and Langham, 1955; Anderson and Hayes, 1956). But hardly any attempt has been made in this country towards a spectrometric study of the background of the place before undertaking such studies. In this laboratory, this spectrometric work has been carried on for the last one year. In the following paper it is desired to report the results of the one-year investigation

on the subject, the variations observed and the possible importance of the results obtained in low-level counting, for instance, in bio-medical tracer technique.

METHODS AND MATERIALS

The studies on the radioactive background of Calcutta were carried out with the help of RIDL Scientillation Spectrometer consisting of a Scaler model no. 16D, B-152; Ratemeter/Electronic Sweep Meter type 114-B, serial B-79; and Scintillation counter No. 43A with interchangeable NaI (thallium activated) crystal of $\frac{1}{2}''$ thickness. The gamma energy distribution was determined under the following conditions: crystal used = NaI $\frac{1}{2}''$ thick; counter voltage = 700 volts; period of sweep = $\frac{1}{4}$ hour; ratemeter scale multiplying factor = 0.5; channel width = 2.0; percentage standard deviation = 10%. A full automatic sweep (without any attenuation) was taken in every case in differential position from 100—0 channel volts, the reset level heliopot being kept at '0'. The graphic record was made with the help of a Honeywell Brown Electronik Recorder automatically.

At the above setting of the instrument, graphic records of the background spectrum was taken throughout the whole year. At the same time, keeping the same instrument settings, scans of I (131) and Cr (51) spectrum were made and their peaks, 364 KeV and 330 KeV respectively were used to calibrate the background spectrum so obtained.

In order to eliminate possible influence of circuit oscillations in the discriminator or elsewhere, and also of photomultiplier noise on the background spectrum, the crystal of the counter was removed from the top of photomultiplier tube and the rest of the counter (consisting of photomultiplier tube, cathode follower, etc.) was wrapped light-tight completely in black paper and a full scan from 100—0 channel level volts was taken keeping the settings of the spectrometer as before.

To study the effect of shielding of the counter on the background spectrum, the counter was inserted in a lead castle with walls $1\frac{1}{2}''$ thick and a full scan from 100-0 channel level volts was made under same instrumental settings. Observations were also made on the variation in background spectra with the changes in atmospheric conditions. Thus an attempt was made to note the variation of intensity below 75 KeV at different times of the day at two hours interval.

After calibration, the energies corresponding to the different peaks in the average spectra obtained were found to tally with those of radium and thorium emanations. To examine this fully the spectra of the important naturally occurring isotopes, viz., Ra (226) in the form of needle and Th (230) as crystal sample were recorded in the same graph containing the background spectrum under same instrumental settings. An attempt was made to trace the sources contributing to the background and the following materials were analysed: (1)

sand from Mogra, (usually used for the building materials here), (2) the silt from the banks of the Ganges, (3) soil samples from the northern and southern parts of the city and (4) the soil from around the building housing the spectrometer. To examine these, a lead chamber having 1 cu. ft. (approximately) of internal volume was constructed with walls 3″ thick. A background tracing with only the counter inside was taken initially and then each of the above samples was packed in the space with the counter placed in the middle. Care was taken to preserve the relative geometry of the counter with respect to the surroundings the same in every case.

RESULTS

The background spectrum consists of two broad energy bands. One such graph is given in Fig. 1. The whole energy spectrum extends from 50 to 275 KeV (Table I). On removing the crystal, a graph was obtained as shown in Fig. 2. This therefore gives the contribution due to circuit oscillations and photomultiplier noise. Comparing Figs. 1 and 2 one can easily recognise the resultant background intensities in this low energy region. Shielding of the counter with lead 1½″ thick cuts off completely the broader higher energy band and attenuates the lower energy region to about ⅓ of its unshielded value (Fig. 3). From Fig. 4, where the Ra (226) and Th (230) graphs are superposed on the background, one finds that the energy peaks corresponding to values round about 230—270 KeV and 105—120 Kev could be associated with the gamma-rays of Ra (226) and Th (230). These elements have been traced in the sand of the building materials and the soil of the city (Figs. 5-9; Table II). From these figures the relative contributions of the sand or of the soil may be clearly seen. Scanning for whole day at two hours intervals showed a variation in the intensity under 55 KeV. The maximum increase of the intensity in this region occurred round about afternoon. Attempts have also been made to indicate this variation together with that of atmospheric temperature and humidity as obtained from the Meteorological office, Alipore.

TABLE I

Results of the gamma ray spectrometric analysis of the background of Calcutta

	Energy range in KeV	Peak values in KeV	Maximum intensity range	Natural radioactive isotope with same energy range
Higher energy band	275–105	275, 245, 230, 185, 175, 170, 160, 135, 125, 105.	160–135	Radium and Thorium family

TABLE II

Samples	Gamma ray energy range in KeV	Maximum intensity range in KeV
1. Sand (from Mogra)	215–50	130–125
2. Soil (from the Ganges)	170–50	145–125
3. Soil (from Lake area)	265–50	140–125
4. Soil (from Science College compound)	175–50	140–130
5. Soil (from S.S.K.M. Hospital compound)	220–50	135–126

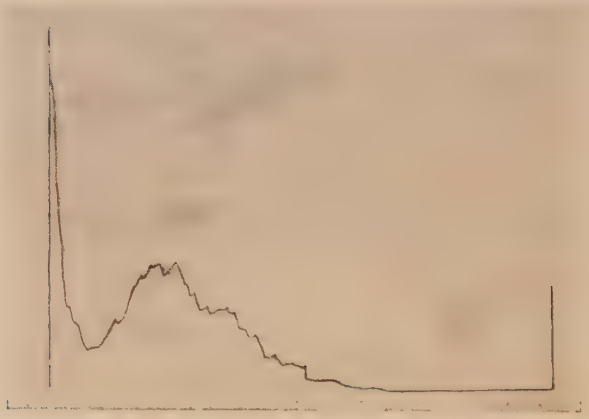

Fig. 1. Shows the radiation background of Calcutta. The scanning was done with the help of RIDL scintillation spectrometer from right to left. The energy of the gamma rays extends from 275–50 KeV.

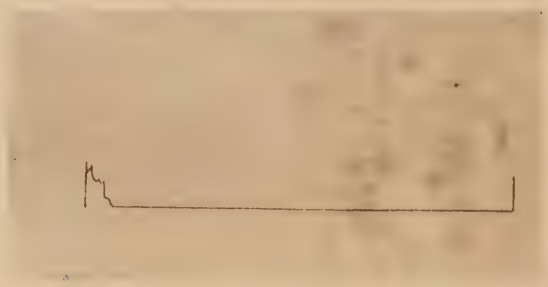

Fig. 2. Shows the contribution due to circuit oscillation and photomultiplier noise. This was taken with the crystal (NaI—thallium activated) removed.

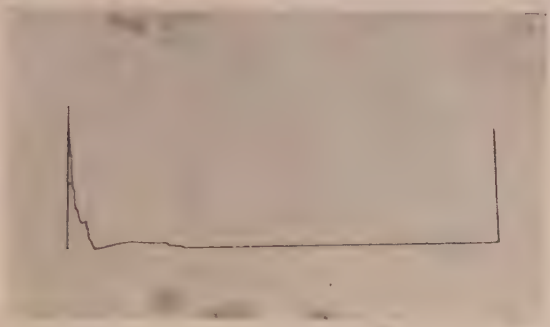

Fig. 3. Indicates the effect of shielding the probe with lead, 1½″ thick. It shows the complete cutting off of the broader higher energy band and attenuation of the lower energy region to about 1/3 of its unshielded value.

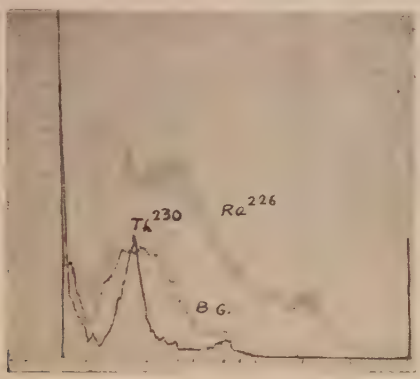

Fig. 4. Shows the superimposition of the tracings due to Ra (226) and Th (230) on the background tracing. Note that the energy peaks of the background could be associated with the gamma rays of radium and thorium family.

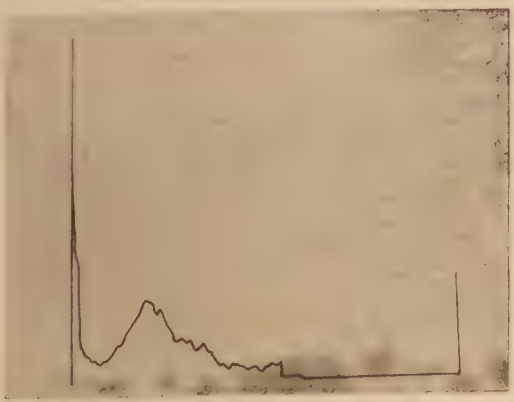

Fig. 5. Shows the gamma ray contribution of soil, collected from lake area (South Calcutta), to the background of the place. The gamma ray energy range due to this extend from 265–50 KeV.

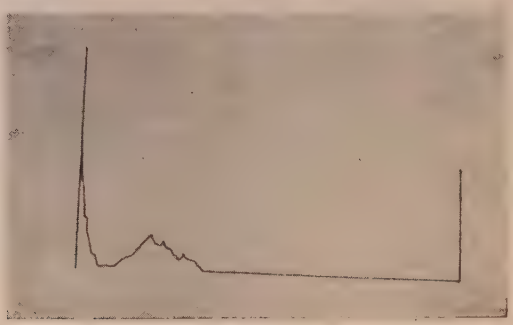

Fig. 6. Shows the gamma ray contribution of soil, collected from Science College (Calcutta) compound, to the background of the place. The gamma ray energy range due to this extends from 175–50 KeV.

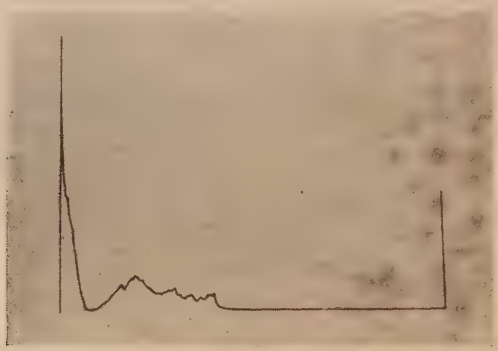

Fig. 7. Shows the gamma ray contribution of sand, collected from Mogra, to the background of the place. The gamma ray energy range due to this extends from 215–50 KeV.

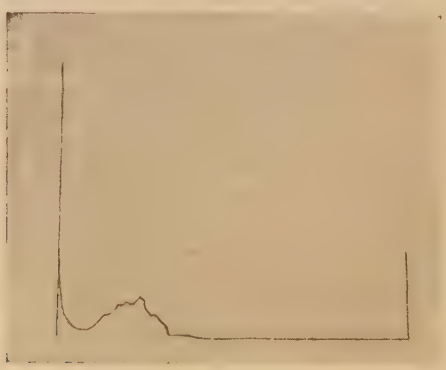

Fig. 8. Shows the gamma ray contribution of soil, collected from the Ganges, to the background of the place. The gamma ray energy range due to this extends from 170–50 KeV.

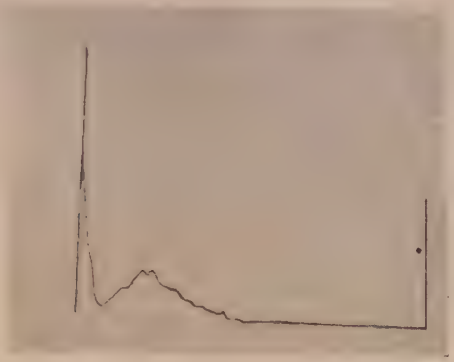

Fig. 9. Shows the gamma ray contribution of soil, collected from the S.S.K.M Hospital compound, to the background of the place. The gamma ray energy range due to this extends from 220–50 KeV.

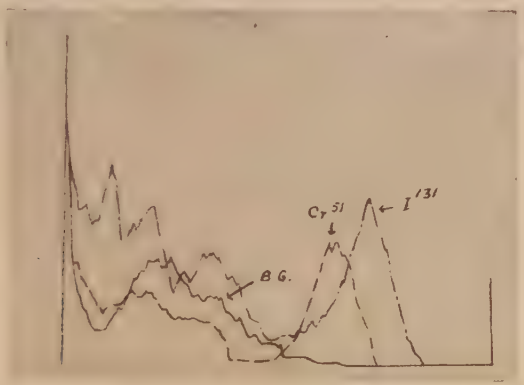

Fig. 10. Shows the superimposition of the three gamma ray spectra due to the background (——), radio-iodine (I–131, — .—) and radio-chromium (Cr-51, — — —). It shows that 50% of the count due to the two isotopes for a particular sample lie above the highest energy limits of the background.

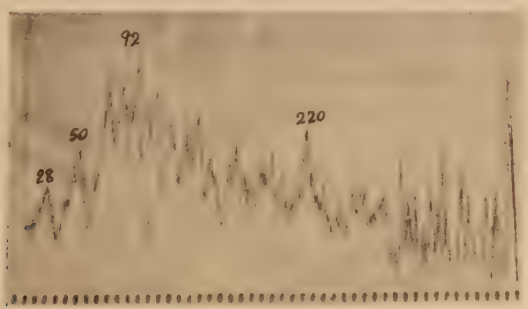

Fig. 11. Shows the background scan carried out at Eindhoven, Holland, with the help of Philips Scintillation Spectrometer. Note the important peaks round about 90 and 220 KeV with possible peaks at 50 and 28 KeV.

Scanning with samples of I (131) and Cr (51) showed that nearly 50% of the counts resulting from particular sample were above the highest energy limits of the background (Fig. 10). This, more or less, was experienced with the other isotopes mentioned above except Fe (55) in which case the radiations were found to be concentrated in the region 90–105 KeV.

A similar background scan was carried out at Eindhoven, Holland, by one of the authors with the help of Philips scintillation spectrometer. The graph thus obtained has important peaks round about 90 and 220 KeV with possible peaks at 28 and 50 KeV, and is similar to the ones obtained here. The intensity of the energy round about 80 to 90 KeV was greatest. The energies in the spectrum would correspond to those found in the members of the uranium and radium family (Fig. 11).

DISCUSSION

The background of Calcutta consists of 2 broad energy bands being contributed by the radioactive substances present in the soil, air and the building materials. The radioactive elements present are those of the Radium and Thorium family.

From the background spectra obtained it is evident that most of the background counts are concentrated in 2 regions—the first between 260 to 135 KeV after which on both sides the counts fall off rapidly and the second region is found to be below 65 KeV. Therefore, in low level counting as with the isotopes for bio-medical tracer work it is necessary only to adjust the channel level of the pulse-height analyser in such a way as to eliminate these regions. The background counts automatically will then fall off without going into the problem of shielding. The best procedure would be to set the channel level potentiometer to a value which corresponds to energies higher than 270 KeV and then expanding the channel window to include the characteristic peak of the isotope being used within the channel window which lies above 275 KeV. The window width preferably should be greater than 2W where 'W' is the recorded half width of the photopeak of the isotope used. In the case of Fe (55) the window should be adjusted near about the trough found between the higher and lower energy bands, i.e., between 65 and 105 KeV. Hence there are 2 regions of low level counting—one above 270 KeV and the other in trough between the higher and lower energy band, i.e. between 60—105 KeV. Thyroid uptake measurements with low doses using the above procedure yielded more reproducible results.

The effect of shielding on the 2 energy bands of the background may at first sight seem to be anomalous as because the lower energy region is expected to be cut off more easily than the higher energy rays on shielding. Possibly, low energy secondary radiations produced by cosmic rays in the material of the shield is responsible for this.

The reason for the variation in the intensity of the low energy region as obtained during certain period of the day cannot be explained satisfactorily right now without further investigation. According to Wait (1937) there is some fluctuation in the gamma-ray content of the atmosphere with a maximum at about noon. This is in agreement with our observation. Further, others (Wilkening, 1952) have reported the variation in the radon and thoron content of the atmosphere with the time of the day. The present investigation points out that this variation in background is restricted mostly to low energy region of the background spectrum. This is a subject matter of further investigation.

ACKNOWLEDGMENT

Grateful thanks are due to Prof. S. D. Chatterjee, D. Sc., F. N. I. and Prof. S. N. Bose. F.R.S.. for their helpful discussion and constant encouragement. Authors also like to acknowledge indebtedness to Major General A. K. Gupta, Director. Institute of Post-graduate Medical Education and Research, for kindly permitting them to carry on the work and also for the facilities obtained.

REFERENCES

Anderson, E. C. and Hayes, F. N., 1955, *Ann. Rev. Nuclear Sc.*, **6**, 303.

Anderson, E. C. and Libby, W. F., 1957, *Adv. Biol. Med. Phys.*, **5**, 385.

Blifford, I. H., Friedman, H., Lockhart, L. B. and Baus, R. A., 1956, *J. Atmospheric and Terrest. Phys.*, **9**, 1.

Hayes, F. N., Anderson, E. C. and Langham, W. H., 1955, *Proc. Intern. Conf. Peaceful uses of Atomic energy.*, **14**, 182.

Johnston, W. H., 1955, Peaceful uses of Atomic Energy International Conf., **14**, 149-54.

Wait, 1937, Terrestrial Magnetism & Atmospheric Electricity., **42**, 1.

Wilkening, M. H., 1952, *Nucleonics.*, **10**, 6, 36.

9

DETERMINATION OF UNLIKE INTERACTIONS FROM BINARY VISCOSITY

I. B. SRIVASTAVA

Indian Association for the Cultivation of Science, Calcutta-32

(*Received, December* 22, 1960)

ABSTRACT.. Experimental viscosity data for the binary gaseous mixtures He–A, Ne–A and H_2–C_3H_8 have been utilised for determining the potential parameters for unlike pairs on the L–J (12 : 6) model. Three different methods have been employed, the first method being applicable only to mixtures exhibiting a maxima with respect to variations in the composition. The other two methods can be used for all gas pairs for which accurate viscosity data are available in a wide temperature range. The parameters thus obtained are tabulated along with those from other sources.

1. INTRODUCTION

Intermolecular potentials between like molecules have been determined with sufficient accuracy by the use of equilibrium and transport properties. For calculating transport properties of pure gases, the force constants used are those determined mainly from viscosity data. There is, however, considerable uncertainty in the values of the force parameters for unlike molecules as determined from the experimental data of inter-diffusion and thermal diffusion, the properties utilised by many workers. This is due to the non-availability of accurate data over a large temperature range and in the case of thermal diffusion there is the additional complication that the higher approximation terms are not negligible. So for the theoretical calculations of the transport properties of mixtures, the force constants for unlike pairs are calculated by the help of some semi-empirical combination rules which are not rigorously true. It is therefore important to be able to derive the unlike interaction parameters by other methods. Recently, Hirschfelder, Taylor and Kihara (1960) have pointed out that the accurate measurements of viscosity of gaseous mixtures as a function of both temperature and concentration can provide a good method of determining the unlike intermolecular forces.

In the present work three different methods have been developed for the determination of the unlike force parameters, provided accurate experimental data are available.

2. THEORY AND FORMULAE

On the basis of the Chapman-Enskog theory, the transport properties have been expressed in terms of a set of reduced collision integrals $\Omega^{(l,s)*}$ which depend

on the law of molecular interaction and are tabulated by Hirschfelder, Curtiss and Bird (1954) for different potential forms. The Lennard-Jones (12 : 6) potential is given by the relation

$$\phi(r) = 4\epsilon\left[\left(\frac{\sigma}{r}\right)^{1} - \left(\frac{\sigma}{r}\right)^{6}\right] \qquad \ldots \quad (1)$$

where $\phi(r)$ is the potential energy between two molecules separated by a distance r, σ is the value of r at $\phi(r) = 0$ and ϵ is the depth of the potential well.

The viscosity of a binary gas mixture η_{mix}, to the first approximation, is given by

$$[\eta_{mix}]_1 = \frac{1+Z_\eta}{X_\eta - Y_\eta} \qquad \ldots \quad (2)$$

with

$$X_\eta = \frac{x_1^2}{\eta_1} + \frac{2x_1x_2}{\eta_{12}} + \frac{x_2^2}{\eta_2}$$

$$Y_\eta = \frac{3}{5} A_{12}^* \left\{ \frac{x_1^2}{\eta_1}\left(\frac{M_1}{M_2}\right) + \frac{2x_1x_2}{\eta_{12}} \cdot \left(\frac{(M_1-M_2)^2}{4M_1M_2}\right) \cdot \left(\frac{(\eta_{12})^2}{\eta_1\eta_2}\right) + \frac{x_2^2}{\eta_2}\left(\frac{M_2}{M_1}\right)\right\}$$

$$Z_\eta = \frac{3}{5} A_{12}^* \left\{ x_1^2 \cdot \left(\frac{M_1}{M_2}\right) + 2x_1x_2\left[\left(\frac{(M_1+M_2)^2}{4M_1M_2}\right)\left(\frac{\eta_{12}}{\eta_1} + \frac{\eta_{12}}{\eta_2}\right) - 1\right] + x_2^2\left(\frac{M_2}{M_1}\right)\right\}$$

x_1, x_2 are the mole fractions, η_1, η_2 the viscosities and M_1, M_2 are the molecular weights of components 1 and 2 respectively. η_{12} is the viscosity of a hypothetical gas given by

$$\eta_{12} \times 10^7 = 266{\cdot}93 \cdot \frac{\sqrt{2M_1M_2T/(M_1+M_2)}}{\sigma_{12}^2 \Omega_{12}^{(2,2)*}(T_{12}^*)} \qquad \ldots \quad (3)$$

3. DETERMINATION OF THE POTENTIAL PARAMETERS

(a) Hirschfelder, *et al.* (1960) have obtained the relation for the maximum or minimum of the viscosity of binary gas mixtures, by differentiating Eq. (2) with respect to x_1 and equating $(d\eta_{mix}/dx_1)$ to zero. The relation for the maximum or minimum viscosity may be written in the form

$$\frac{(\eta_{mix})_{max}}{(\eta_1\eta_2)^{1/2}} = \frac{\beta_c(\beta - \beta^{-1}) - 2\beta_c}{\beta_c^2 - 1}$$

where $$\beta = (\eta_1/\eta_2)^{1/2} \quad \ldots (4)$$

and $$\beta_c = K(2R)^{-1}(1-\alpha+f) \quad \ldots (5)$$

with $$R = (M_1+M_2)^{1/2}/(4M_1M_2)^{1/4}$$

$$K = \frac{\sigma_1\sigma_2\sqrt{\Omega_{11}^{(2,2)*}(T^*).\Omega_{22}^{(2,2)*}(T^*)}}{\sigma_{12}^2\Omega_{12}^{(2,2)*}(T_{12}^*)} \quad \ldots (6)$$

$$\alpha = 3/5\ A_{12}^* \text{ and } f^2 = (1-\alpha)^2+4\alpha R^4$$

Here for getting maximum in the viscosity β must lie between β_c and β_c^{-1}.

The maximum value of experimental viscosity is obtained from the graph of η_{mix} against x_1 for each temperature. This is substituted in Eq. (4) along with the experimental values of η_1 and η_2 and the equation solved for β_c. Let the values of β_c at two temperatures T_1, T_2 be $(\beta_c)_1$, $(\beta_c)_2$. Then using the subscripts 1 and 2 to denote the quantities at temperatures T_1 and T_2 we get from eqns. (5) and (6)

$$(\beta_c)_1/(\beta_c)_2 = \frac{K_1}{K_2} \cdot \left(\frac{(1-\alpha_1+f_1)}{(1-\alpha_2+f_2)} \right) \quad \ldots (7)$$

and $$K_1/K_2 = \left(\frac{\Omega_{12}^{(2,2)*}(T_2^*)}{\Omega_{12}^{(2,2)*}(T_1^*)} \right) \cdot \left(\frac{\Omega_{11}^{(2,2)*}(T_1^*)\ \Omega_{22}^{(2,2)*}(T_1^*)}{\Omega_{11}^{(2,2)*}(T_2^*)\ \Omega_{22}^{(2,2)*}(T_2^*)} \right) \quad \ldots (8)$$

With the help of the Eqns. (7) and (8) and the tabulations of Hirschfelder *et al.* (1954), for the collision integrals and A_{12}^*, the ratio $(\beta_c)_1/(\beta_c)_2$ is calculated for a number of arbitrarily chosen values of ϵ_{12}/k and a graph drawn for $(\beta_c)_1/(\beta_c)_2$ versus ϵ_{12}/k. The desired value of ϵ_{12}/k for the gas pair is then read from the graph corresponding to the value of $(\beta_c)_1/(\beta_c)_2$ determined from Eq. (4). The value of σ_{12} can be calculated easily with the help of Eqns. (5) and (6) by using this value of ϵ_{12}/k.

In the present work the force parameters for He–A and H_2–C_3H_8 interaction have been calculated by this method. For He–A, the recent data of Rietveld, *et al.* (1953) at temperatures 291·1°K, 229·5°K and 192·5°K could be successfully combined to give three sets of ϵ_{12}/k and σ_{12} values, the mean of which is recorded in Table I. Only one set of force constants of H_2–C_3H_8 could be obtained as the data at only two temperatures 500°K and 550°K taken from Trautz and Kurz (1931) could be used successfully.

This method can give accurate and consistent values for force constants, provided accurate experimental data are available even at two temperatures but it is applicable to only those binary gas mixtures which show maxima or minima in viscosity at some concentration.

(b) *Method of Intersection* :

The graphical methods of intersection and Lennard-Jones translation discussed in detail by Srivastava and Srivastava (1959) can be successfully used for obtaining the unlike force parameters on the L–J (12 : 6) potential from the data on viscosity of gas mixtures. For this purpose Eq. (2) is solved for η_{12} giving

$$\eta_{12} = \frac{-b \pm \sqrt{b^2 - 4ac}}{2a} \qquad \ldots (9)$$

where $$a = \frac{6}{5} A_{12}^* \cdot \left(\frac{x_1 x_2}{\eta_1 \eta_2} \right) \left(\frac{(M_1+M_2)^2}{4M_1M_2} \right) \cdot (\eta_{mix} - \eta_1 - \eta_2)$$

$$b = \frac{3}{5} A_{12}^* \left[2x_1x_2 + x_1^2 \cdot \left(\frac{M_1}{M_2} \right) \cdot \left(\frac{\eta_{mix}}{\eta_1} \right) + x_2^2 \cdot \left(\frac{M_2}{M_1} \right) \left(\frac{\eta_{mix}}{\eta_2} \right) - x_1^2 \cdot \left(\frac{M_1}{M_2} \right) - x_2^2 \left(\frac{M_2}{M_1} \right) \right] + \eta_{mix} \left(\frac{x_1^2}{\eta_1} + \frac{x_2^2}{\eta_2} \right) - 1$$

and

$$c = 2x_1x_2\eta_{mix}$$

Now by substituting the experimental values of η_1, η_2 and η_{mix} at any temperature, η_{12} is obtained in terms of A^*_{12} which is a temperature dependent function and whose values are tabulated by Hirschfelder, *et al.* (1954). Then η_{12} is calculated for one temperature by substituting the value of A^*_{12} corresponding to any arbitrarily chosen value of ϵ_{12}/k and by using this η_{12} value the corresponding σ_{12} value can be obtained from Eq. (3). In this way a set of ϵ_{12}/k and σ_{12} values are calculated at one temperature. The same process is repeated for getting sets of values of ϵ_{12}/k and σ_{12} at other temperatures. Graphs are then plotted for ϵ_{12}/k against σ_{12} at each temperature. The intersection point gives the required values of ϵ_{12}/k and σ_{12} for the gas pair.

This method has been utilised to determine the force parameters for the gas pairs He–A and Ne–A. There is usually some uncertainty in exactly locating the intersection point when the experimental data are not very accurate. In view of the extensive data on mixture viscosities, however, this method can serve as a useful supplement to other methods for determining unlike force parameters.

(c) *Translation Method* :

If experimental data are available in a large range of temperature, the translation method can be applied with the following device. From table, A^*_{12} is found to vary very slowly with T^* and can therefore be taken to be constant over a very small range of T^*, say, for a change of about 3%. It is thus possible

to calculate A^*_{12} at any temperature with sufficient accuracy by using the value of ϵ_{12}/k obtained from the combination rule, as the true value of ϵ_{12}/k is not likely to differ from the combination rule values by more than about 3%. Knowing A^*_{12} in this manner, η_{12} can be determined from Eq. (9) by utilising the experimental values of η_{mix}, η_1 and η_2. Thus knowing η_{12} at different temperatures and using Eq. (3), the Lennard-Jones translation method can be applied for getting ϵ_{12}/k and σ_{12}. In case this value of ϵ_{12}/k is much different from the value previously selected from the combination rule, the process can be repeated by using this refined value of ϵ_{12}/k.

This method is used here for determining the force parameters for the gas pairs He–A and Ne–A.

4. RESULTS

The force parameters determined by these methods are given in Table I along with those determined from other sources.

TABLE I

Unlike Force Parameters on the L–J (12 : 6) model

Gas Pair	Force Parameters	Present work			Previous work			Ref. for data
		From maximum viscosity	Intersection method	Translation method	Comb. rules	From inter-diffusion	From Thermal diffusion	
He–A	ϵ_{12}/k°K	36.97	36.97	36.9	35.6	33.8[a]	37.91[b]	A
	σ_{12}Å	2.96	2.985	3.028	2.997	2.99	3.025	
Ne–A	ϵ_{12}/k°K	..	69.0	66.37	66.6	64.5[c]	67.6[b]	B
	σ_{12}Å	..	2.943	2.932	3.104	3.098	3.079	
H_2–C_3H_8	ϵ_{12}/k°K	103.8	..	..	98.25	..	..	C
	σ_{12}Å	4.019	..	..	3.988	..	..	

(A) Rietveld and Itterbeek (1953).
(B) Trautz and Binkele (1930).
(C) Trautz and Kurz (1931)
(*a*) Srivastava and Srivastava (1959)
(*b*) Saxena (1955)
(*c*) Srivastava (1959).

5. DISCUSSION

It will be seen from the table that the three methods employed here give quite consistent values of the unlike force parameters which agree well with the values obtained from the combination rules. This shows clearly that the viscosity data on mixtures of gases can be employed to give quite reliable values for the unlike interaction parameters. Unfortunately the large amount of exist-

ing data on mixture viscosities had never been directly utilised so far for calculating the unlike force parameters. The present investigations show that this is quite feasible and desirable.

The values of the unlike parameters obtained by others using thermal diffusion data show good agreement with the present determinations, but those obtained from inter-diffusion data exhibit noticeable discrepancies. It is worth nothing that in the evaluation of the unlike force parameters from inter-diffusion data, the force parameters for like interactions were not utilised, while all the other methods cited here depend upon the accuracy of the force parameters for pure components also.

ACKNOWLEDGMENTS

The author is grateful to Prof. B. N. Srivastava, D.Sc., F.N.I., for suggesting the problem and many helpful discussions throughout the progress of this work.

REFERENCES

Hirschfelder, J. O., Curtiss, C. F. and Bird, R. B., 1954, Molecular Theory of Gases and Liquids, John Wiley and Sons, Inc., New York.

Hirschfelder, J. O., Taylor, M. H. and Kihara, T., 1960, Report, WIS-OOR-2?.

Rietveld, A. O., Van Itterbeek, A. and Van Der Berg, G. J., 1953, *Physica*, **19**, 517.

Saxena, S. C., 1955, *Ind. Jour. Phys.*, **29**, 131.

Srivastava, B. N. and Srivastava, K. P., 1959, *J. Chem. Phys.*, **30**, 984.

Srivastava, K. P., 1959, *Physica*, **25**, 571.

Trautz, M., and Binkele, H. E., 1930, *Ann. Physik*, **5**, 561.

Trautz, M. and Kurz, F., 1931, *Ann. Physik*, **9**, 981.

10

A LOW PRESSURE EXPANSION CLOUD CHAMBER

M. RAMA RAO

Saha Institute of Nuclear Physics, Calcutta-9

(*Received, December* 17, 1960)

ABSTRACT. A pressure defined expansion cloud chamber has been constructed and operated satisfactorily up to total pressures of 5 cm of Hg. The best track conditions for different total pressures as a function of the expansion ratio have been determined and discussed using ethyl, *n*-butyl and iso-amyl alcohols as condensant vapour and argon as permanent gas. Photographs of Po^{210}-$_\alpha$ tracks taken at 5 cm. of Hg with iso-amyl alcohol and argon mixture are presented.

1. INTRODUCTION

A low pressure cloud chamber finds special applications in the study of uranium fission and of other low energy interactions of heavy charged particles with matter. Where the ranges of the observed track lengths in a gas at atmospheric pressure in such interactions are so short that the track lengths are not measurable, advantage of the fact that lowering of pressure of the gas-vapour mixture in the active volume of the chamber "magnifies" the ranges of the particles has been utilised to get greater details of the interaction. Thus, Joliot (1934) has operated a low pressure cloud chamber in order to study the mechanism by which heavy ions, resulting from radioactive decay, lose their energy. R. G. Mills (1953) has used a mechanical expansion mechanism to actuate a low pressure cloud chamber and operated at pressures of 4.5 cm in the investigation of the stopping power of He and water vapour.

Operation of a cloud chamber at low pressures involves additional difficulties which are not in common with cloud chambers generally used over a wide range of pressures. Lowering of the initial pressure is achieved by reducing the partial pressure of the permanent gas. The gamma coefficient of the vapour-gas mixture becomes smaller and in order to obtain the necessary supersaturation for condensation of the vapour on ions higher expansion ratios are needed. At the same time lowering of the partial pressures of the permanent gas restricts the uniform diffusion of the condensing vapour on growing drops. This effect becomes important in the low pressure region as the vapour-gas mixture has a low heat capacity. The low heat capacity and the large temperature variations involved for obtaining the necessary supersaturation result in an intensive and fast heat exchange between the filling mixture and the chamber walls leading

to the lowering of the supersaturation and a consequent shortening of the sensitive time. For this reason a fast expansion mechanism is of extreme importance in the operation of a low pressure cloud chamber.

The higher expansion ratios needed to work the cloud chamber at low pressures as mentioned earlier introduces the undesirable effects of turbulence motion of the gas molecules within the chamber, thereby resulting in the distortions of the tracks. This situation can be avoided by a suitable choice of the gas-vapour mixture such that good quality of tracks can be obtained for a given pressure with a relatively smaller and conveniently reproducible expansion ratio. Further the choice of the gas-vapour mixture has a vital role to play with reference to the particular mode of operation in which we are interested. In all randomly operated cloud chambers operating at low as well as high pressures, water vapour or some form of alcohol is used as a condensant vapour, together with a non-condensible gas like air or argon. Since the cloud chamber is intended to be triggered by an internal counter controlled mechanism such that the desired events can be selected and photographed by suitably running an open counter in the proportional region (Hodson *et al.*, 1950), a selective choice of the gas-vapour mixture has to be made so as to make a compromise between obtaining good tracks and at the same time operating the counter within for the same gas-vapour filling. In counter operation the production of gas multiplication depends on the electrons remaining freely mobile and electron attachment must be avoided. For this reason oxygen and water vapour have been excluded and our choice has been narrowed down to the study of several alcohols as condensants and argon as the non-condensible gas.

This paper describes the constructional details of a pressure defined expansion cloud chamber. Results of an investigation on the adequate choice of the gas-vapour mixture for obtaining best track conditions at different initial total pressurs in relation to the expansion ratios are also presented.

2. CONSTRUCTIONAL DETAILS OF THE CHAMBER

The cloud chamber constructed is a pressure defined expansion chamber of the rubber diaphragm type and the assembly of the different components of the apparatus is shown in Fig. 1.

The front chamber which constitutes the active volume of the chamber is made of a perspex cylinder 10 inches i.d. and 2 inches in height, the wall thickness being 1/4 inch. A circular glass plate 1/2 inch thick covering the top of the perspex cylinder forms the window of the main chamber which faces the camera mounted vertically upwards for taking stereoscopic pictures. A thin rubber diaphragm 1/32 inch thick isolates the main chamber volume from a pan-shaped back chamber made of copper. The back chamber is separated from the vacuum ballast having a volume approx. 10 litres by means of an expan-

sion valve which is normally closed under gravity. The expansion valve used is an Edwards 1 inch bore high vacuum magnetic isolation valve operated on 200 volts D.C. The connecting links between the chamber and the inlet of the expansion valve and that between outlet of the expansion valve and the ballast are copper pipes of short lengths 1 inch in diameter. The vacuum ballast is evacuated by means of a Cenco high vacuum pump and maintained roughly at 10^{-3} mm of Hg. which is the limiting pressure of the pump.

Initially the back chamber is maintained at a pressure slightly higher than that in the main chamber, such that the rubber diaphragm is blown forward against the perforated disc, thereby diminishing the active volume of the main chamber. Expansion is initiated by energising the magnet, and when the magnet valve opens, the sudden release of pressure in the back chamber by getting a direct communication with the vacuum ballast forces the rubber diaphragm downwards until it comes to rest against the perforated backing plate. This sudden change in the relative positions of the rubber diaphragm followed by a corresponding change in the volume of the main chamber causes the expansion of the gas in the main chamber volume and undergoes an adiabatic cooling. The adjustment of the amount of the expansion is controlled by changing the position of the backing plate. The backing plate is made of 3/32 inch brass plate with a number of uniformly spaced 1/8 inch drill holes all over and is rigidly

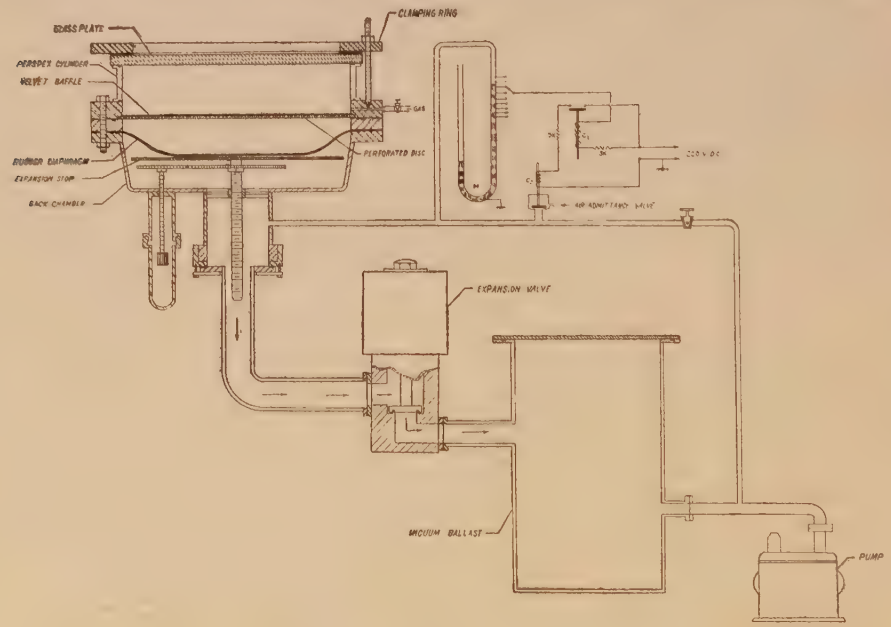

Fig. 1. Constructional details of the cloud chamber.

screwed on to a threaded rod capable of vertical motion in the back chamber. The motion of this rod can be conveniently regulated from outside, without

any major dismantling of the components of the apparatus, by means of a mutually coupled gear system as shown in Fig. 1. The perforated disc at the top is similar to the one at the bottom and is covered with a screen wire mesh which is faced with a black velvet cloth to form a uniform photographic background. The drill holes in the top plate together with the wire mesh and the pores in the velvet will define the stream lines of motion of the gas and reduce the turbulence of the gas molecules when the rubber diaphragm is being pulled down so that the tracks are free from distortion.

The underside of the glass plate is coated with a ring of Aquadag to make the surface electrically conductive. A sweep field of +45 volts is applied between this coating and the base of the chamber, which serves to remove the background ions produced by the tracks during the preceeding expansion. For illumination of the tracks, two Mazda flash tubes, F.A.2 rated at 500 Joules are used. Two banks of condensers each 64 μF normally charged to 2000 volts are discharged through the flash tubes by a spark coil. The spark coil is triggered by discharging a small condenser through the primary of the coil. Cylindrical lenses are used to collimate the light from the flashing units, into a parallel fan-shaped beam limited in height by diaphragms in order to avoid direct light reaching the top and the bottom of the chamber.

3. AUTOMATIC PRESSURE CONTROL DEVICE

The equipment shown at the right hand top of Fig. 1 is an automatic device for setting back the pressure in the back chamber to the same desired level after every expansion. The mechanism can be understood as follows: As soon as the magnet valve opens, expansion of the chamber takes place and there is a lowering of the back chamber pressure owing to its communication with the ballast which is maintained at a sufficiently low pressure. A little later the magnet current is short circuited by closing a relay included in the electronic sequence arrangement (not shown here) which returns the valve to its normal position and thus isolating the back chamber from the vacuum ballast. Simultaneously, the pressure difference in the back chamber is communicated to a mercury manometer M, through an auxiliary connection, taken from the bottom of the chamber. There are a number of contact points of tungsten fused into the right hand limb of the manometer at regular intervals and by changing the point of contact, the pressure in the back chamber can be cut off at discrete levels. In the present position of the mercury level as indicated in the manometer representing the state of affairs immediately after expansion, the relay coil C_1 is energised and the relay is pulled down, thus interrupting the current in the coil C_2 of the air admittance valve. This valve is the Edwards magnetic air admittance valve 1/16 inch bore, maintained closed magnetically against a spring which opens the valve to atmosphere when the current is switched off.

Thus, when the current in the magnet coil is switched off air is admitted through the valve into the back chamber and simultaneously the mercury level in the manometer is pushed down to a level just below the variable contact point. At this stage the relay coil C_1 is de-energised and the current path for the air admittance valve is restored thus closing the magnet valve and preventing any further admittance of air.

In practice, however, after running for several days a thin conducting coating is formed on the inner glass walls of the mercury manometer owing to impurities in the mercury so that the spacing between the several variable contact points is electrically bridged up and the purpose of discretely cutting off the pressures is not achieved. This is avoided by cleaning the tungsten contacts and also rinsing the manometer with dilute Hydroflouric acid and also filtering the mercury at intervals.

4. RESULTS AND DISCUSSION

The main chamber was completely evacuated initially and simultaneously the back chamber was also evacuated to prevent implosion of the rubber diaphragm. 5 c.c. of dehydrated alcohol was injected into the main chamber and the desired total pressure in the working chamber has been set up by introducing argon whose flow is regulated by a needle valve. The total pressures in the main chamber are recorded by means of a mercury manometer, connected to

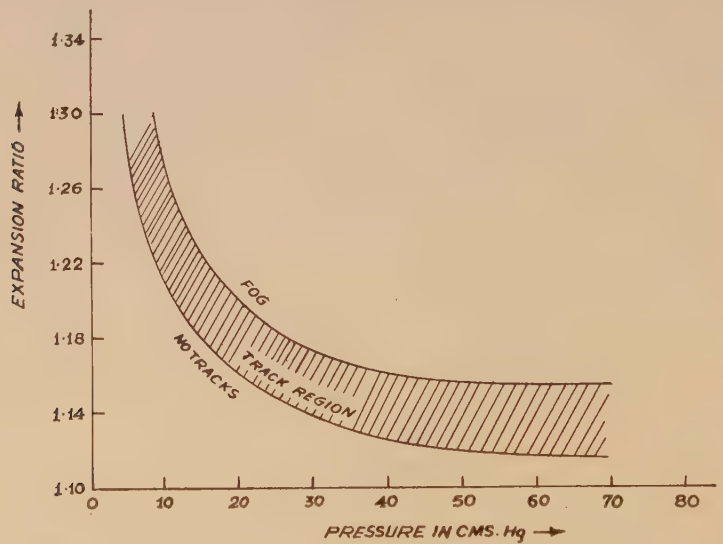

Fig. 2. A typical curve showing the variation of expansion ratio with initial total pressures for any alcohol showing the ion and cloud limits. This particular curve is that for iso-amyl alcohol.

the main chamber, not shown in Fig. 1. The expansion ratio, defined as the ratio of the initial to the final pressures, has been adjusted by defining the position of the stopping plate. The best track conditions were visually and photo-

graphically determined for different initial total pressures, each time the desired total pressure being built up by leaking in argon into the working chamber.

Fig. 2 presents the variation of expansion ratio with total pressures obtained for iso-amyl alcohol and argon.

The shaded area represents the region of track formation. The best track conditions, however, lie close to the lower boundary of this region. As we go towards the interior of this region and away, the tracks are masked with a background fog and the quality of tracks deteriorates. Observations have been carried out with different alcohols with a view to choose a suitable gas-vapour mixture for operating the chamber at very low pressures with conveniently reproducible expansion ratios. The results of investigation obtained with ethyl, *n*-butyl, iso-amyl alcohols are shown in Fig. 3 and in each of these curves only the best track conditions are presented.

In the above series of experiments $Po^{210}-\alpha$ tracks were visually observed and photographed at different pressures. The source in the form of a foil prepared in the laboratory from used randon needles is mounted on a perspex base and supported inside the chamber from the wall of the perspex cylinder.

The interpretation of the general trend of the curves can be better understood from the following considerations.

The supersaturation produced as a result of expansion is given as (Das Gupta and Ghosh, 1946)

$$S = \frac{p_1}{p_2}\,(1+\epsilon)^{\gamma} \qquad \ldots \quad (1)$$

Where $(1+\epsilon)$ is the expansion ratio p_1, p_2 are the saturation pressures at the initial and final temperatures.

γ = ratio of specific heats of the complex gaseous mixture in the chamber. If p_g and p_v be the partial pressures of the gas and vapour with the corresponding γ's, γ_g and γ_v, γ for the composite mixture is given by the formula due to Richarz (1906) as

$$\frac{1}{\gamma-1} = \frac{1}{\gamma_g-1}\cdot\frac{p_g}{P} + \frac{1}{\gamma_v-1}\cdot\frac{p_v}{P} \qquad \ldots \quad (2)$$

where P is the total pressure equal to (p_g+p_v).

It is seen from equation 2 that when the total pressure P is decreased by diminishing the gas pressure p_g, p_v/P increases while p_g/P remains practically the same for $p_g >> p_v$ as a result the value of γ decreases. For a given expansion ratio the fall of temperature is therefore less and the supersaturation produced smaller. Thus, one needs a higher expansion ratio to attain the same degree of supersaturation. The curves plotted in Fig. 3 for the best rack conditions with different alcohol vapours show a functional dependence of the expansion ratio on the total initial pressures,

It is further observed by an intercomparison of the curves drawn for different alcohols that there is a finite dependence of the expansion ratio on the molecular weights of the alcohols involved. The heavier the alcohol, smaller is the expansion ratio needed to bring about the same degree of supersaturation for a

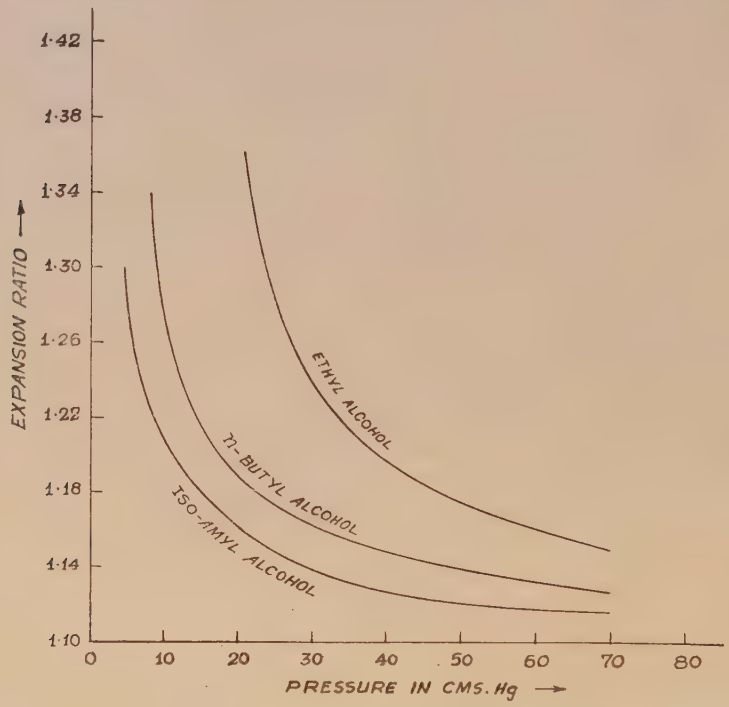

Fig. 3. Variation of expansion ratio with initial total pressures for best track conditions with different alcohols.

given pressure. Flood (1934) found that the value of supersaturation at the ion limit or cloud limit depends strongly upon the type of vapour used in the chamber. Thus, iso-amyl alcohol with a molecular weight 88.15 requires a much smaller expansion ratio than *n*-butyl alcohol whose molecular weight is 74.12.

It was shown by Powell (1928) that when the partial pressures of a condensible vapour becomes a large fraction of the whole pressure, many factors operate which restrict the growth of supersaturation. The supersaturation reached is much smaller than that deduced from adiabatic expansion. The effect is attributed to the evaporation of hot vapours from the free liquid surface in the chamber. Joliot (1934) has shown that the working expansion ratio increases from 1·305 at atmospheric pressure to about 2 when only saturated water vapour remains. It is thus apparent that the operation of a conventional cloud chamber with pure alcohols is a matter of considerable difficulty and the permanent gas plays an important role in its operation.

In the present set of observations it is seen that by using heavier alcohol, the initial total working pressure can be pushed down to lower pressures than with the lighter alcohols. In case of iso-amyl alcohol it is as low as 5 cm. This is perhaps on account of the fact that for a given total pressure, the vapour pressure contributed by the heavier alcohol is in a smaller proportion to the total pressure than for the lighter alcohols with the result that the permanent gas which is in considerable quantity plays its role for proper condensation at conveniently reproducible expansion ratios.

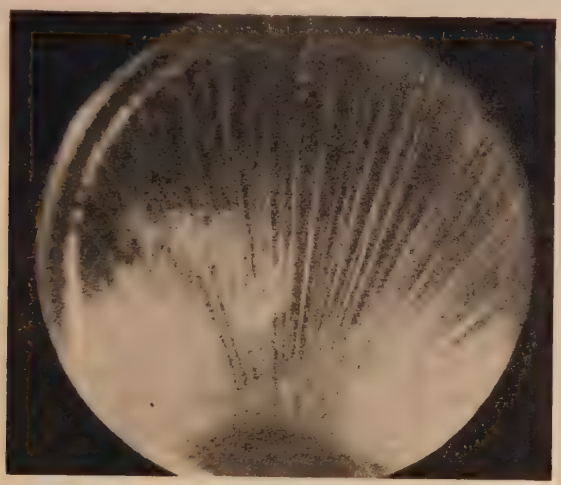

Fig. 4. A typical photograph of $P_0^{210} - \alpha$ tracks at 5 cm of Hg using iso-amyl alcohol and argon.

Fig. 4 shows a typical photograph of $P_0^{210}-\alpha$ tracks obtained at 5 cm of Hg using iso-amyl alcohol and argon as the filling mixture and the tracks can be seen stretched to lengths extending over the entire diameter of the chamber. Thus, the advantages of such magnified track lengths can be appreciated when one has to work with fission fragments or such other reaction products with low energy which have ranges of only few millimeters at atmospheric pressures.

ACKNOWLEDGMENTS

The author is indebted to Prof. B. D. Nag Chaudhuri, Director, Saha Institute of Nuclear Physics, for suggesting the problem and continued guidance through the progress of the work. Grateful thanks are due to Prof. D. N. Kundu for his helpful suggestions and discussions. In the earlier stages Mr. A. P. Patro was associated with the work, to whom thanks are also due.

REFERENCES

Das Gupta, N. N. and Ghosh, S. K., 1946, *Rev. Mod. Phys.*, **18**, 225.
Flood, C. H., 1934, *Z. Phys. Chem.*, **170**, 294.
Hodson, A. L., Loria, A. and Ryder, N. V., 1950, *Phil. Mag.*, **41**, 826.
Joliot, F., 1934, *J. Phys. Radium*, **5**, 216.
Mills, R. G., 1953, *Rev. Sci. Instr.*, **24**, 1041.
Powell, C. F., 1928, *Proc. Roy. Soc.*, A, **119**, 553.
Richarz, F., 1906, *Ann. d. Physik*, **19**, 639.

Letters to the Editor

The Board of Editors will not hold itself responsible for opinions expressed in the letters published in this section. The notes containing reports of new work communicated for this section should not contain many figures and should not exceed 500 words in length. The contributions must reach the Assistant Editor not later than the 15th of the second month preceding that of the issue in which the letter is to appear. No proof will be sent to the authors.

1

EQUIVALENT PRESSURE CONCEPT IN CROSSED ELECTRIC AND MAGNETIC FIELD IN ELECTRODELESS DISCHARGE

S. N. SEN AND A. K. GHOSH

DEPARTMENT OF PHYSICS, JADAVPUR UNIVERSITY, CALCUTTA-32

(*Received December* 29, 1960)

Wehrli (1922) calculated the effect of a magnetic field on the breakdown condition of a gas by assuming that λ, the mean free path of the electron, is constant for all the electrons and under the action of the magnetic field the electrons will describe a cycloidal path and the mean free path λ will change to λ' such that

$$\lambda' = \lambda \left[1 - \frac{eH^2\lambda}{8Em}\right] \quad \ldots \quad (1)$$

Where H is the magnetic field in Gauss, e and m are the charge and mass of the electron and E is the breakdown voltage per centimetre length of the discharge tube. Hence the effect of magnetic field is equivalent to an increase of pressure P to P_e such that

$$P_e = \frac{P}{\left[1 - \frac{eH^2\lambda}{8Em}\right]} \quad \ldots \quad (2)$$

Blevin and Haydon (1958) arrived at a new expression for equivalent pressure by calculating the electron mass energy and drift velocity in a magnetic field and P_e in their case is given by

$$P_e = P\sqrt{1 + \frac{CH^2}{P^2}} \quad \ldots \quad (3)$$

where $$C = \left(\frac{e}{m} \cdot \frac{L}{u}\right)^2;$$

L is the mean free path of the electron in the gas at a pressure of 1 m.m. and u is the velocity of the electron. It can be seen from equation (3) that

$$P_e = P\sqrt{1 + \frac{e^2}{m^2} \cdot \frac{L^2}{u^2} \cdot \frac{H^2}{P^2}}$$

and if it can assumed that $\frac{1}{2}mu^2 \quad eEd$ where d is the length of the discharge tube then

$$\left.\begin{aligned} \frac{P_e}{P} &= \sqrt{1 + \frac{1}{2} \cdot \frac{e}{m} \cdot \frac{L^2H^2}{P^2Ed}} \quad \text{(Blevin and Haydon's formula)} \\ \text{and from Eqn. (2)} \\ \frac{P_e}{P} &= \frac{1}{\left[1 - \frac{eH^2L}{8PEm}\right]} \quad \text{(Wehrli's formula)} \end{aligned}\right\} \quad \ldots \quad (4)$$

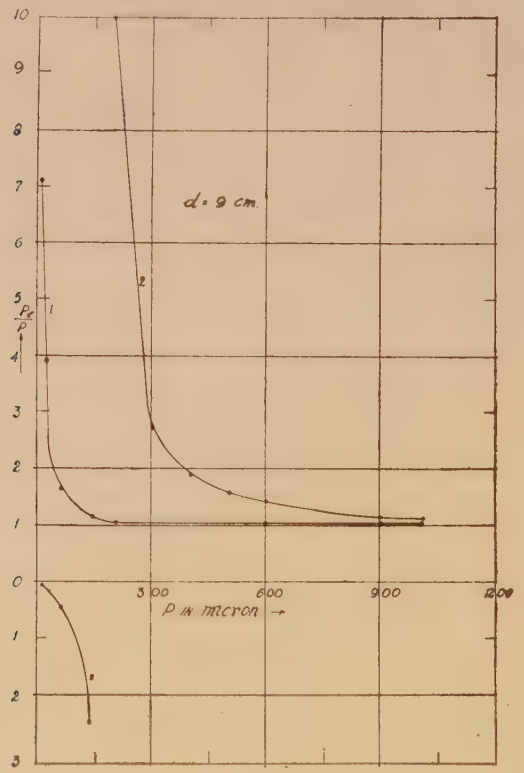

Fig. 1

We have recently measured the breakdown potential in air in crossed electric and magnetic field within the pressure range 1×10^{-3} to 1 mm of Hg, the discharge being excited by means of a 10 KV transformer. The magnetic field has been varied from 50 Gauss to 2000 Gauss and three discharge tubes of length

9 cm, 22·5 cm. and 26·5 cm. have been used. From the measured breakdown potential data, the values of P_e/P have been calculated using both the expressions in Eqn. (4) where the magnetic field has been taken as 100 Gauss and in Figs. (1) and (2), P_e/P has been plotted against the corresponding pressure. From the curves it appears that the relative change of pressure as obtained from Blevin and Haydon's formula is large when the pressure is very small, that is below 60μ of Hg. and then drops suddenly and becomes insignificant above 200μ. On the other hand, Wehrli's formula predicts negative values of equivalent pressure at low pressure which is anomalous. At about 220μ of Hg, P_e/P becomes very large in the case of Wehrli's formula and then drops suddenly and both the curves become asymptotic to the straight line $P_e/P = 1$ at higher pressures. Values of P_e/P calculated for higher magnetic fields also give similar nature of the curve. If calculations for the equivalent pressure be made using Wehrli's formula for

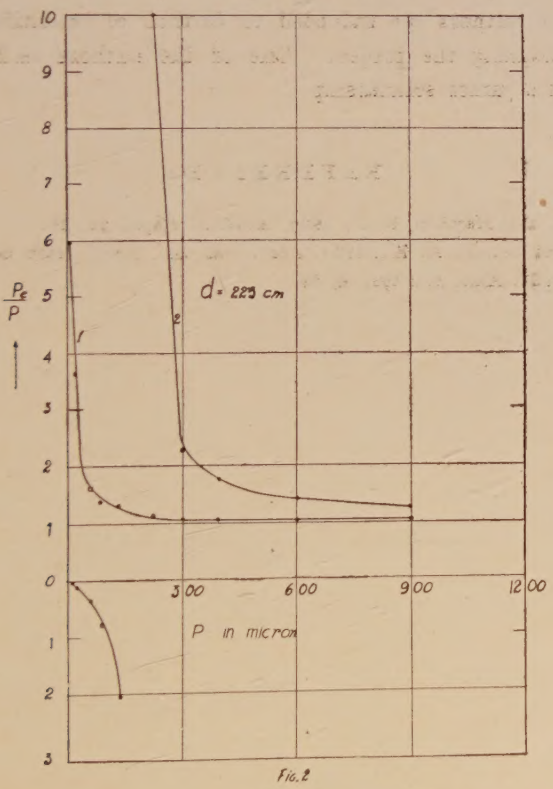

Fig. 2

small values of magnetic field of the order of 15 to 30 Gauss then it predicts positive values of P_e at low pressure. Thus at low pressure, Wehrli's formula becomes valid only if the magnetic field is small. It can be seen from Fig. 1, that both the curves almost provide the same value of P_e/P above 900μ of Hg.

and above 200μ the change of P_e/P is insignificant. But in our experiment it has been noted that the effect of magnetic field on breakdown potential is dominant at higher pressure also. Thus it can be concluded that both the above expressions for P_e are of limited applicability and the concept of equivalent pressure alone cannot explain all the observed results. So far the variation of γ, Townsend's second coefficient in a magnetic field, has been neglected, but we have recently deduced an expression for variation of γ with (E/P) (Sen and Ghosh 1961) and it is hoped that the incorporation of variation of γ with H along with equivalent pressure concept will explain the observed changes better.

ACKNOWLEDGMENT

The present work forms of a programme on scheme on "Electrical discharge through gases and vapours and its investigation by microwave probe and optical method" and the authors are indebted to Council of Scientific and Industrial Research for financing the project. One of the authors (A.K.G.) is grateful for the award of a junior scholarship.

REFERENCES

Blevin, H. A. and Hayden, S. C., 1958, *Aust. J. Phys.*, **11**, 18.
Sen, S. N. and Ghosh, A. K., 1961, *Proc. Ind. Sci. Cong.*, 48th Session.
Wehrli, M., 1922, *Ann. d. Phys.*, **4**, 69.

CONTENTS

Indian Journal of Physics Vol. 35, No. 2 February, 1961

PRINTED BY KALIPADA MUKHERJEE, EKA PRESS, 204/1, B. T. ROAD, CALCUTTA-35
PUBLISHED BY THE REGISTRAR, INDIAN ASSOCIATION FOR THE CULTIVATION OF SCIENCE
2 & 3, LADY WILLINGDON ROAD, CALCUTTA-32